Ambient-mediated wetting on smooth surfaces

Ambient-mediated wetting on smooth surfaces

Daniel Orejon[1,2 *], Junho Oh[3], Daniel J. Preston[4], Xiao Yan[5], Soumyadip Sett[6], Yasuyuki Takata[1,2], Nenad Miljkovic[2,7] and Khellil Sefiane[1]

[1]School of Engineering, Institute for Multiscale Thermofluids, The University of Edinburgh, Edinburgh EH9 3FD, Scotland, UK

[2]International Institute for Carbon-Neutral Energy Research (WPI-I2CNER), Kyushu University, 744 Motooka, Nishi-ku, Fukuoka 819-0395, Japan

[3]Department of Mechanical Engineering, BK21 FOUR ERICA-ACE Center, Hanyang University, Ansan, Gyeonggi 15588, Republic of Korea

[4]Department of Mechanical Engineering, Rice University, Houston, Texas 77005, US

[5]Mechanical and Aerospace Engineering, The Hong Kong University of Science and Technology, Hong Kong 999077, China

[6]Mechanical Engineering, Indian Institute of Technology Gandhinagar, Gujarat 382355, India

[7]Department of Mechanical Science & Engineering, University of Illinois at Urbana–Champaign, Urbana, IL 61801, US

Abstract:

A consensus was built in the first half of the 20th century, which was further debated more than 3 decades ago, that the wettability and condensation mechanisms on smooth solid surfaces are modified by the adsorption of organic contaminants present in the environment. Recently, disagreement has formed about this topic once again, as many researchers have overlooked contamination due to its difficulty to eliminate. For example, the intrinsic wettability of rare earth oxides has been reported to be hydrophobic and non-wetting to water. These materials were subsequently shown to display dropwise condensation with steam. Nonetheless, follow on research demonstrated that the intrinsic wettability of rare earth oxides is hydrophilic and wetting to water, and that a transition to hydrophobicity occurs in a matter of hours-to-days as a consequence of the adsorption of volatile organic compounds from the ambient environment. The adsorption mechanisms, kinetics, and selectivity of these volatile organic compounds are empirically known to be functions of the substrate material and structure. However, these mechanisms, which govern the surface wettability, remain poorly understood. In this contribution, we introduce current research demonstrating the different intrinsic wettability of metals, rare earth oxides, and other smooth materials, showing that they are intrinsically hydrophilic. Then we provide details on research focusing on the wetting to non-wetting transition to hydrophobicity due to adsorption of volatile organic compounds. A state-of-the-art figure of merit mapping the wettability of different smooth solid surfaces to ambient exposure and surface carbon content is developed. In addition, we analyse recent works that address the wetting transitions so to shed light on how such processes affect droplet pinning and lateral adhesion. We then conclude with objective perspectives about research on wetting to non-wetting transitions on smooth solid surfaces in an attempt to raise awareness regarding surface *contamination* within the engineering, interfacial science, and physical chemistry domains.

*Corresponding author: d.orejon@ed.ac.uk

Keywords: Volatile Organic Compounds, Atmosphere Mediated Wettability, Surface Physicalchemistry, Contact Angle Hysteresis, Adsorption

Introduction:

Wetting and spreading of liquids on solid surfaces or liquid-like surfaces are relevant to many medical, biological, thermal management, microfluidics, industrial, and agricultural applications [1-3]. The interactions between liquid films or droplets and surfaces are determined by the physicochemical properties of the solid surface, the nature of the liquid, and the surrounding environment [4-7]. In order to elucidate such interactions, researchers have made use of the equilibrium and/or apparent contact angle θ_0 as a metric to classify whether a surface likes (-philic) water (hydro-), i.e., hydrophilic or θ_0 for water < 90°, or whether it dislikes (-phobic) water (hydro-), i.e., hydrophobic or θ_0 for water > 90°. The contact angle adopted on a solid surface θ_0 depends on the different solid-gas γ_{sg}, liquid-gas γ_{lg} and solid-liquid γ_{sl} binary surface tensions or interfacial interactions as per the force balance established at the triple phase contact line (TPCL) by the Young or the Young-Dupré equation, **Eq.1** 1 [8, 9]. It is worth noting that the Young-Dupré equation is valid for a smooth, chemically homogeneous, ideal surfaces in thermodynamic equilibrium, i.e., immediately after droplet deposition [10]:

$$\cos\theta_0 = \frac{\gamma_{sg} - \gamma_{sl}}{\gamma_{lg}}. \quad (1)$$

Based on **Eq. 1**, the wettability of metals and non-metal solid surfaces such as gold, silver, rhodium and palladium [11, 12], as well as ceria [13] and supported graphene [14] amongst others, has been classified as hydrophobic and predicted to enable dropwise condensation of steam [15]. However, recent work has shown evidence that reinforces these surfaces to be classified as intrinsic hydrophilic [16]. Newly fabricated surfaces, or surfaces analysed immediately after polishing and/or after cleaning with strong acids (HCl), strong bases (NaOH) or via air, oxygen or argon plasma cleaning, typically show hydrophilic behaviour, i.e., a water droplet spreads over the surface adopting contact angles below 40° [16-19]. It is after the surfaces are exposed to the ambient that their wettability is modified and becomes less wetting. Such a change in the wetting behaviour has then been attributed to the gradual adsorption of airborne volatile organic compounds (VOCs) or semi-volatile organic compounds (sVOCs) present in the ambient [16-19].

VOCs and sVOCs are typically hydrocarbons (HCs), such as alkanes, olefins, halogens, and/or oxygen containing molecules [20], which are present in the environment in very small quantities, i.e., parts per billion (ppb) or parts per trillion (ppt). These chemicals end up in the atmosphere as a consequence of manmade related practises such as industrial processes [21], combustion and electricity generation [22], urban emissions [23], cooking [24], and biochemical processes [25]; as well as natural sources such as marine phytoplankton[26], livestock and plant life [21, 27-29]. VOCs are ubiquitous and have been reported to be present in the surrounding environment [23, 30, 31]. They adsorb onto the ocean surface [22, 32], as well as onto solid surfaces [16] even under high vacuum environments [33]. VOCs vary in nature depending on the length of the chain of the carbon group, their polarity, as well as their termination, including alkanes, alkenes, aromatic hydrocarbons, and alcohols, amongst others [34] . On a solid surface, the gradual increase of sVOCs and/or VOCs presence have been demonstrated by mapping the temporal carbon concentration on the surface outermost layer via surface chemical characterisation techniques such as X-Ray Photoelectron Spectroscopy (XPS) [16, 19, 20], time of flight secondary ion mass spectroscopy (ToF-SIMS)[19, 20], and Electron Diffraction Spectroscopy (EDS) [35]. The non-polar nature of these VOCs is responsible for masking the

intrinsic hydrophilicity of solid surfaces by decreasing the surface energy of the outermost layer exposed to gas or liquid interactions. It is this masking effect, which empowers the transition from wetting to non-wetting as the surfaces are exposed to the environment [16, 18]. Moreover, recent work has demonstrated that the presence of metallic nano- or hierarchical micro-/nano-structures on the substrate acts to generate superhydrophobicity and dropwise condensation, highlighting the potential of VOCs to passively coat rationally designed metallic surfaces where otherwise hydrophilic or superhydrophilic wetting behaviour would be anticipated [20, 35].

Despite the breadth of research carried out on this topic over the past century, the adsorption mechanisms, chemisorption or physisorption, the adsorption kinetics and/or selectivity, as well as the specific VOCs contribution to the change on the surface physical chemistry related to wettability, are not clearly understood. The expected wettability transition as smooth surfaces are exposed to VOCs or HCs can be exemplified as the schematics presented in **Fig. 1**:

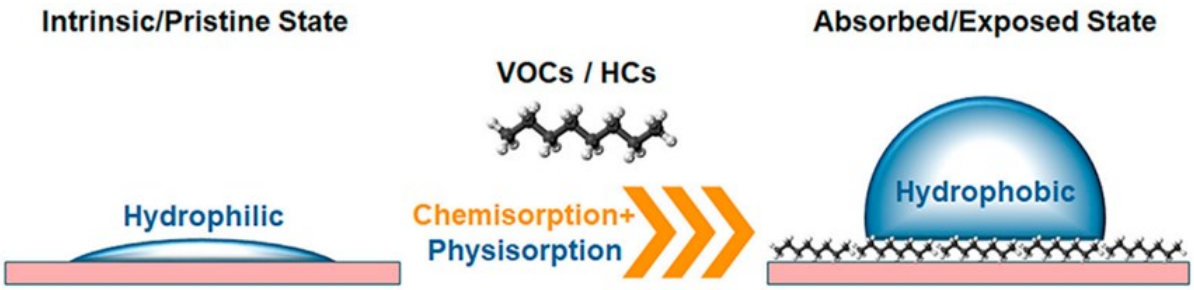

Fig. 1 – Schematics of the hydrophilic to hydrophobic wettability transition [19]. Schematics not to scale. **(left)** Hydrophilic or intrinsic/pristine state immediately after fabrication and/or plasma cleaning where a water droplet (blue) wets the surface. **(right)** Hydrophobic or adsorbed/exposed state where the VOCs and/or HCs mask the intrinsic wettability as they adsorb via chemisorption and/or physisorption. Copyright 2022 Elsevier Inc.

The first aim of this review is to provide the reader with the necessary overview and awareness on the effect of anthropogenic VOCs on solid surfaces and the role they play in masking the intrinsic hydrophilicity of high surface energy solids, and its impact on the wetting to non-wetting transitions via ambient exposure. A second aim is to raise further awareness as well as to regain acknowledgment from the surface science, physical chemistry, and engineering communities, on the importance of such phenomena, when designing uncoated solid surfaces for specific applications. We achieve these aims by firstly introducing earlier works in the literature where the effect of VOCs on wettability was acknowledged, albeit in a not systematic way. Second, we provide systematic investigations mapping the wettability of smooth solid surfaces as a function of ambient exposure carried out in the past decade, as well as introduce efforts by the scientific community to elucidate the composition of the solid surface outermost layer. A figure of merit summarising most of the literature on the wettability of solid surfaces to date *versus* carbon content is further drawn. Thirdly, both plausible adsorption mechanisms looking at the different adsorption models in the literature, as well connotations of VOCs adsorption on droplet pinning, are further introduced and discussed. This review concludes with a summary and outlook on the effect of VOCs on wetting and pinning on solid surfaces and discusses the potential of this passive atmospheric coating approach for understanding and empowering high droplet mobility as well as effective surface design for a number of applications.

Wettability of intrinsically hydrophilic surfaces

The effect of organic contamination from the ambient on wetting, adhesion, friction, and other properties of inorganic solids, was acknowledged as early as the beginning of the 20th century, with most studies reporting on the intrinsic hydrophilic wettability of clean metal surfaces via pure liquid spreading [36-39]. At that time, it was further conveyed that it is the exposure of the surfaces to the ambient what results in measurable contact angles, which can be as high as 100°, as the outermost layer of a solid surface adsorbs organic contaminants present in the environment [40, 41]. Despite such established understanding, in the early 1960s, a disagreement initiated which focused on the intrinsic hydrophobicity of noble metals such as gold. Two leading groups those of Robert Erb [11] and Malcolm L. White [42] supported the idea of intrinsic hydrophobicity of metals, while Bewig and Zisman opposed [41]. In spite of being aware of the effect of organic contamination on wetting, Erb carried out inclined plane advancing and receding contact angle measurements on different metal surfaces immediately after cleaning via cellulose tissue soaked in ethanol [11]. Depending on the material tested, advancing and receding contact angles ranged between 30° and 50° on mechanically polished palladium, and 46° and 85° on a gold layer deposited via bright electroplating. The hydrophobicity of gold was also supported by White, who did not report any quantitative values on contact angles, but concluded that it is the oxide layer what empowers hydrophilicity while pure gold shows hydrophobicity [42]. Hydrophobic wettability observations on gold reported by Erb and by White were adopted by Frederick Fowkes [43] in his seminal work, who concluded that only the spreading coefficient making use of the dispersion forces contributing to surface tension should be used in order to predict the wettability of such surfaces.

During the same time period, Bewig and Zisman contested these observations by demonstrating that clean metals, i.e., free of adsorbed hydrocarbons and oxides, become completely wetted by water [41]. Their experiments were methodologically designed and carried out within a gas purification apparatus while making use of a metal specimen heat cell, which avoided the exposure of the surface to volatile organic compounds (VOCs) or to any other contaminants. They concluded that complete spreading of a water ensues on oxide-free metal surfaces as these have higher surface energy than metal oxides. They also concluded that the absence of complete spreading should be attributed to the presence of contamination, which is hydrophobic in nature [41, 44]. We note that to date, direct measurements of solid-liquid surface tension or interfacial energy are challenging and difficult to acquire; although a recent technique making use of a solid-liquid meniscus has the potential to overcome such difficulties [45].

In addition to the aforementioned works focusing on water droplet contact angle as a metric to determine the wettability of solid surfaces, the characterisation of a solid surface either as hydrophilic or hydrophobic can be, to some extent, related to the condensation mechanism (filmwise or dropwise) ensuing on the surface. The different surfaces fabricated and tested by Erb provided different condensation behaviour depending on the material as well as the condensation time [11]. Both gold and silver empowered dropwise condensation behaviour over a 14 day period. Interestingly, rhodium initially displayed filmwise condensation followed by an increase in the effective area displaying dropwise condensation of up to 80% after 6 days, with 100% area-coverage of dropwise condensation after 14 days. Other materials such as chromium, copper-nickel alloy and stainless steel, showed filmwise behaviour over 90% of the condensing area after 2 days of experiments [11]. Thereafter, Tennyson Smith pioneered a qualitative and quantitative investigation on the

building of a monolayer of carbon on the surface by providing a systematic study on both wettability of clean surfaces as well as the non-wetting behaviour reported on exposed ones [46]. By applying Auger Electron Spectroscopy (AES), Smith found that all surfaces displayed some content of carbon on the surface and were able to empower dropwise condensation, i.e., hydrophobic wetting behaviour, while filmwise condensation ensued on carbon free surfaces. This work stressed the importance of the cleaning procedure to unveil the actual intrinsic wettability of high surface energy metals, in this case gold. Shortly after, the review of James Westwater represents one of the very first works summarising and opening again the debate on the different condensation mechanisms either as filmwise or dropwise, when comparing a clean surface and an ambient exposed surface where carbon-containing compounds have been adsorbed on the latter [47].

The scientific community so far acknowledges surface contamination via VOCs adsorption as a nuisance rather than a phenomenon and/or a mechanism that is intrinsic to surface wettability and that deserves research effort and further attention. This is further supported by the wide range of wettability values reported by different research groups for the very same solid surfaces depending on the cleaning procedure as well as the composition of the ambient. For example, contact angles as low as 16° are found on silicon oxide wafers cleaned by piranha solution [48], and as high as 57° reported after cleaning in an ultrasonic bath with ethanol [49]. Besides influencing wetting, the different liquid-solid interactions and/or condensation behaviours reported have been attributed to the intrinsic wettability of the solid surface instead of the actual presence of contaminants and/or VOCs adsorbed onto the surface, which lacks scientific accuracy and betterment. To provide a more direct account on the effect of ambient exposure on the change in physicochemical properties of the outermost surface with focus on wettability, we next introduce different works in the literature reporting on the wetting to non-wetting transitions taking place on smooth solid surfaces as a consequence of ambient exposure.

Wetting to non-wetting transitions

Earlier works investigating the wettability of solids surfaces as a function of surface carbon content are introduced next, which in chronological order are those of Strohmeier [17], Takeda *et al.*[18], and Kim *et al*.[50]. Strohmeier made use of oxygen plasma treatment to effectively remove carbon/volatile organic compounds (VOCs) contamination from an aluminium foil resulting in a relatively clean surface, which had higher wetting than the uncleaned one. After oxygen plasma cleaning, the wetting behaviour decayed in time as a consequence of carbon-based component adsorption as elucidated via XPS [17]. The adsorption of carbon-based components onto the outermost layer of the surface was qualitatively and quantitatively demonstrated by the presence of a C 1s carbon peak at a binding energy of ca. 285 eV. The intensity of the peak could be, to some extent, related to the amount of HCs/VOCs adsorbed. In addition to removing carbon/VOCs contamination from a surface, Strohmeier also acknowledged that oxygen plasma treatment could further modify or functionalise the surface by increasing the oxide layer thickness, which in turn may modify the wetting behaviour. To exemplify the effect of contaminants on the wettability of solid surfaces, the temporal evolution of the contact angle during exposure to ambient air was reported (**Fig. 2a**). A linear increase in in the contact angle from ~ 5° to ~ 55° was observed within 3 days of exposure while for further exposure the contact angle saturates at ~ 60°. However, the systematic tracking of the surface chemical composition evolution versus exposure time was not carried out and only XPS spectra immediately after cleaning and after 2 weeks of exposure were provided as shown in **Fig. 2c**, which yielded a relative quantitative carbon increase from 7% to 45%.

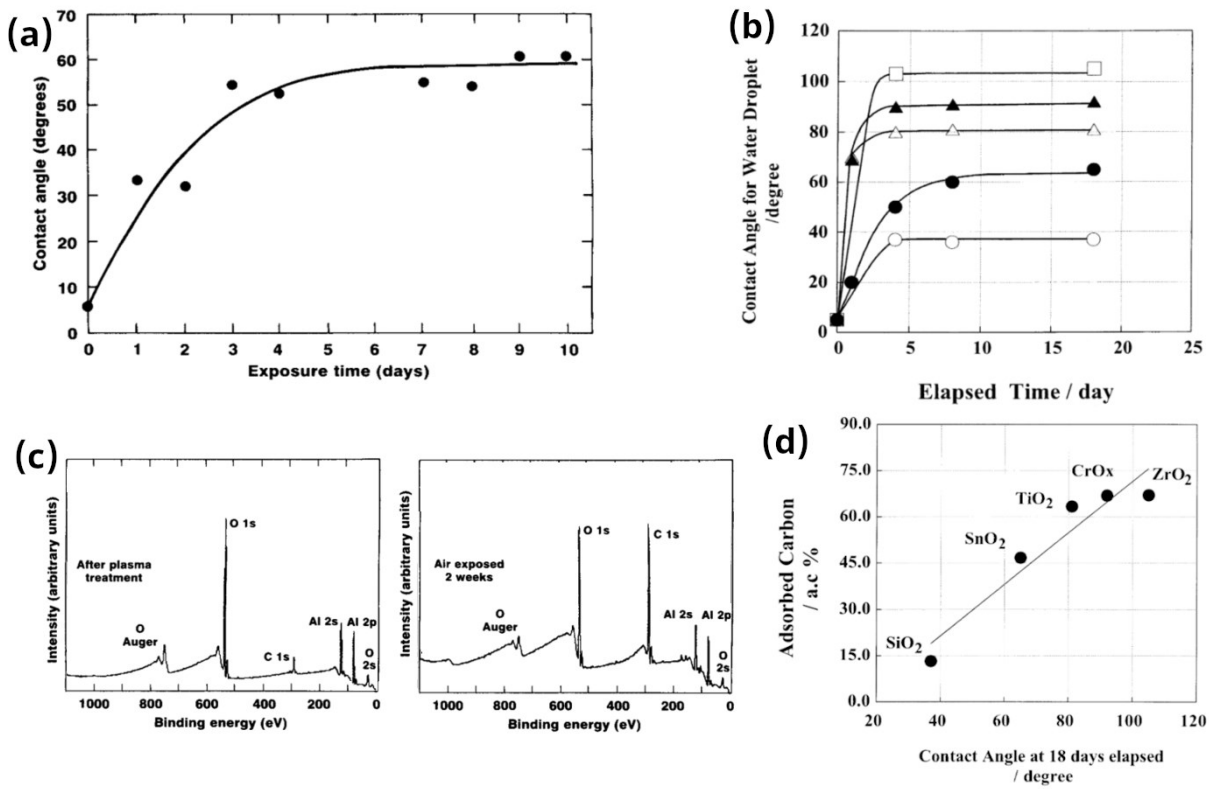

Figure 2 – Wettability and chemical composition and/or carbon content at the outermost layer. (a) Contact angle (deg) versus exposure time (days) [17]. Copyright 1989 American Institute of Physics. **(b)** Contact angle (deg) versus exposure time (days) for (empty circles) SiO_2, (solid circles) SnO_2, (empty triangles) TiO_2, (solid triangles), CrO_x and (empty squares) ZrO_2 [18]. Copyright 1999 Elsevier B.V. **(c)** X-Ray Photoelectron Spectroscopy (XPS)

representing the intensity (arbitrary units) versus binding energy (eV) on aluminium foil (left) after oxygen plasma treatment and (right) after 2 weeks of exposure with the Carbon peak C 1s at 285 eV [17]. Copyright 1989 American Institute of Physics. **(d)** Carbon content adsorbed (%) versus contact angle (deg) at 18 days of exposure [18]. We note the initial linear increase in the contact angle followed by a plateau after several days of exposure with a different final contact angles as a function of both the material and the amount of adsorbed carbon content. Copyright 1999 Elsevier B.V.

Almost a decade later, Takeda *et al.* systematically studied the effect of ambient exposure and chemical surface composition on the wettability of different 40-nm thick metal oxide films such as: SiO_2, SnO_2, TiO_2, CrO_x and ZrO_2, which were deposited via reactive magnetron sputtering [18]. Since the surface energy of oxides is typically high, contact angles in the wetting regime were reported immediately after film deposition. While a saturation value of the contact angle was reported after 5 days of laboratory ambient exposure. Both the different dynamics of the contact angle increase in time as well as the final contact angle values were highlighted and shown to vary from 40° on SiO_2 to ~100° on ZrO_2 (**Fig. 2b**). Besides the different dynamics observed during the evolution of the contact angle; Takeda *et al.* also reported on the different magnitudes of adsorbed carbon (%) after 18 days (**Fig. 2d**), which clearly demonstrated the different affinity of carbon/VOCs to each material. It is hence anticipated that the kinetics and selectivity of VOCs adsorption onto solid surfaces are a strongly related to the type of material they are adsorbing onto. Takeda *et al.* further carried out negative ToF-SIMS, which was able to identify the amount of hydroxyl/OH groups on the surface when coupled with XPS. They proposed that the amount of carbon adsorbed onto the prepared films was also function of the amount of hydroxyl OH groups on the surface [18]. Few year later, Kim *et al.* carried out an investigation using aluminium, steel use stainless (SUS), and copper. A clear decrease in the contact angle as well as in carbon content measured via XPS were reported after atmospheric plasma jet treatment, which is in agreement with the earlier aforementioned works [50].

Although the aforementioned works provide some quantification of the relation between surface wettability and the amount of carbon present at the outermost surface layer; these investigations lack systematic temporal quantification of the wettability and surface chemical composition. To overcome this deficiency, Preston *et al.* carried out a thorough systematic physicochemical study looking at both the wettability and the chemical composition of the outermost surface as a function of the ambient exposure time. They investigated the wettability of two rare earth oxides (holmia Ho_2O_3 and ceria CeO_2), a transition metal (gold Au), and a metalloid oxide (silica SiO_2), after cleaning with argon plasma [16]. After plasma cleaning, the wettability of the tested rare earth oxides as well as that of gold and silica, was hydrophilic with contact angles ~ 5°. In particular, the wettability of CeO_2 and Ho_2O_3 transitioned from wetting/hydrophilic (~ 5°) for clean/carbon-free surfaces to non-wetting/hydrophobic (~ 90°) for exposed surfaces in the span of 96 hours (**Figs. 3a & 3b**) [16, 51]. Moreover, other materials such as silica and gold also reduced their wetting behaviour, although the contact angles reported were still within the hydrophilic regime [16, 47]. The quantification of the dynamic evolution of the advancing contact angle as a function of the surface ambient exposure time to laboratory conditions after argon plasma cleaning were reported (**Fig. 3c**). Moreover, quantitative information about the surface atomic percent carbon (%C) as a function of time (hours) detected via XPS on all 4 samples was also elucidated and reported (**Fig. 3d**).

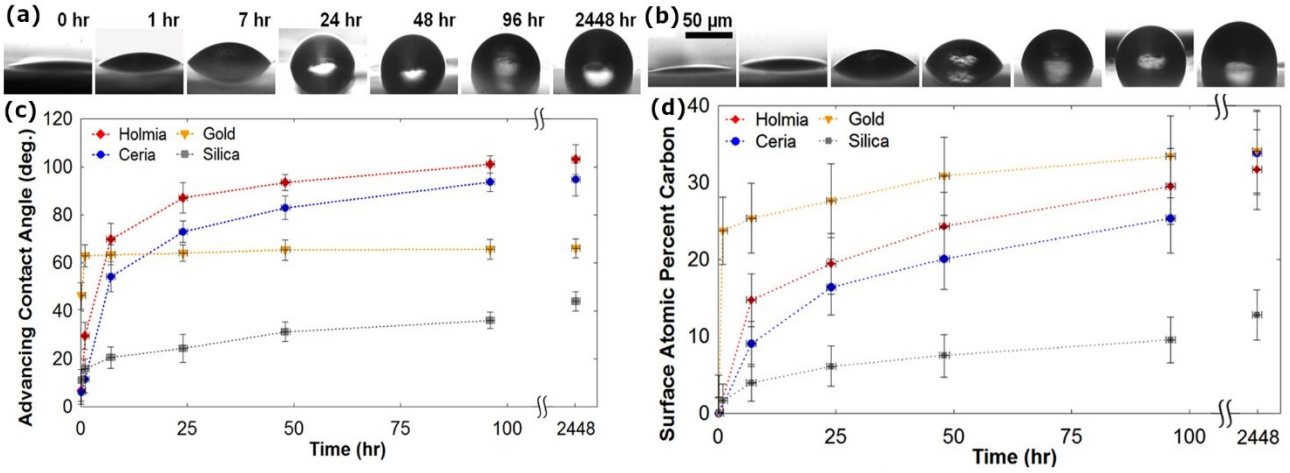

Figure 3 – Wetting to non-wetting transitions and surface carbon content as a function of ambient exposure time from Preston *et al.* [16]. Droplet profile photographs for varying exposure times (hours) for **(a)** holmia Ho_2O_3 and **(b)** ceria CeO_2. Scale bars are 50 µm. **(c)** Advancing contact angle (deg) as a function of time (hours) and **(d)** surface atomic percent of carbon/VOCs (%C) as a function of time (hours), for (red diamonds) holmia Ho_2O_3, (blue circles) CeO_2, (orange down-triangles) gold and (grey squares) silica SiO_2. Copyright 2014 American Institute of Physics.

First, we draw the readers' attention to the rather good qualitative agreement in the evolution of the contact angle versus exposure time reported in **Fig. 2a**, **Fig. 2b** and **Fig. 3c**, where an initial linear increase followed by a logarithmic asymptotic trend ensues [16-18]. Second, we note the different quantitative values reported for the final contact angle, which are functions of the specific material [16-18]. Third, we also highlight the rather similar qualitative trends reported on both the change in contact angle as well as the change in surface atomic percent of carbon as a function of time for the different surfaces tested when comparing **Figs. 3c** and **3d**. In the case of gold, a sharp increase in the content of carbon from ~ 0% to 25%, with this latter value near its saturation value of 35%, was observed within the first hour of exposure, which is in good agreement with the increase in contact angle to its saturation/asymptotic value of ~ 60° within the same timeframe. For silica and both rare earth oxides (holmia Ho_2O_3 and ceria CeO_2), a smoother logarithmic asymptotic trend can reproduce the evolution of both the advancing contact angle as well as the carbon surface atomic percent as a function of time. These results highlight the different kinetics and selectivity of VOCs adsorbing onto solid surfaces depending on the material, which eventually governs surface wettability as well as transition to non-wetting. The gradual transition from hydrophilic to hydrophobic reported in **Fig. 3(c)** is attributed to VOC adsorption as exemplified by the amount of surface carbon (%C) increase in a logarithmic asymptotic trend in **Fig. 3(d)** detected via XPS as function of time (hours) [16]. Of interest are also the receding contact angles reported for both holmia and ceria along with their advancing contact angles as a function of carbon content (**Fig. 4b** and **4b**) [16]. Since the difference between the advancing and receding contact angles ultimately dictates the contact angle hysteresis, defined as: $CAH = \theta_a - \theta_r$, such results will be utilised in the subsequent section to provide further insights and estimation on the effects of ambient exposure and VOCs carbon coverage on droplet pinning.

Next, we introduce the work of Lundy *et al.*, who targeted one rare earth oxide at two different oxidation states in ceria (III) Ce_2O_3 and ceria (IV) CeO_2, two transition metal oxides in zirconia (ZrO_2) and hafnia (HfO_2), and a metalloid oxide silica in SiO_2 [51]. Lundy's work aimed to better understand the wettability of a solid surface as a function of the oxidation state as well as for other transition metal oxides. Similar to the findings reported by Preston *et al.*, all surfaces studied by Lundy *et al.* showed hydrophilic behaviour after argon plasma cleaning. Although the latter work reported higher advancing contact angles with different quantitative values between 40° and 60° for ceria (III) Ce_2O_3, ceria (IV) CeO_2, zirconia ZrO_2 and hafnia HfO_2, while an advancing contact angle as low as 10° was found for silica right after cleaning, as reported in **Fig. 4a** and **Fig. 4b**. We note that results reported in **Fig. 4a** were obtained after exposing the surfaces to laboratory ambient conditions while in **Fig. 4b** surfaces were exposed to a perfluorononane C_9F_{20} saturated environment in a desiccator, which may explain the different quantitative values reported for the contact angles as well as the carbon content in the case of ceria (IV). The expected less wetting behaviour function of exposure time was confirmed for both ceria (III) and ceria (IV) when looking at the advancing contact angle, while the receding contact angle was not affected with all values ~15° and independent of the exposure time (**Fig. 4a**). The logarithmic asymptotic trends reported for the advancing contact angle for both ceria (III) and ceria (IV) in **Fig. 4a** agree qualitatively with those observed for the carbon surface coverage as it will be discussed later in a subsection focusing on adsorption models. No apparent differences were observed when comparing the two rear earth oxides terminations, i.e., ceria (III) and ceria (IV). When comparing the different oxides, the wettabilities for hafnia and zirconia behaved in a similar quantitative and qualitative manner under a perfluorononane C_9F_{20} environment as shown in **Fig. 4b**. Results on silica introduced in **Fig. 4b** also demonstrates the validity of Lundy's work as per the agreement with the work of Preston *et al.* despite the different atmospheres studied [16]. Of notable interest is the continuous increase in the receding contact angle for silica up to 35° while the rest of the substrates did not reach values above 15°. Such a difference in the receding contact angles reported will eventually play a role on droplet pinning as it will be introduced and discussed in a later subsection. A different atmosphere, that of nonane C_9H_{20}, was also explored by Lundy *et al.*, which produced relatively higher advancing contact angles and no major differences on the receding contact angles (see Figure 7a and Figure 7b from the work of Lundy *et al.*[51]). Further, a direct linear increasing relationship was drawn in **Fig. 4c** between the advancing contact angle and the element electronegativity difference defined as $\Delta\chi = (M - O)$ where M and O stand for the electronegativity of the element and that of the oxygen respectively. Results from the work of Preston *et al.* [16], Takeda *et al.* [18], and Azimi *et al.* [13], were further included in **Fig. 4c** to allow for a more direct quantitative comparison and to support the proposed relation. A summary on the reported saturation advancing and receding contact angles for hafnia, zirconia, ceria (III) and silica was further included in the work of Lundy *et al.* (**Fig. 4d)** [51]. The saturated advancing contact angles ranged between 70° and 90°, while the receding contact angles were fixed near 20°, which suggests a contact angle hysteresis (CAH), defined as the difference between the advancing and receding contact angles as CAH = θ_a - θ_a, on these surfaces of 50° or more. However, if these samples were to be annealed at 900 °C, a two-fold or three-fold increase in the receding contact angle could be achieved brining the hysteresis of these surfaces to values below 40° and as low as 15° in the case of silica.

Considerations on the CAH differences as a consequence of ambient exposure on droplet pinning will be introduced and discussed in a later subsection.

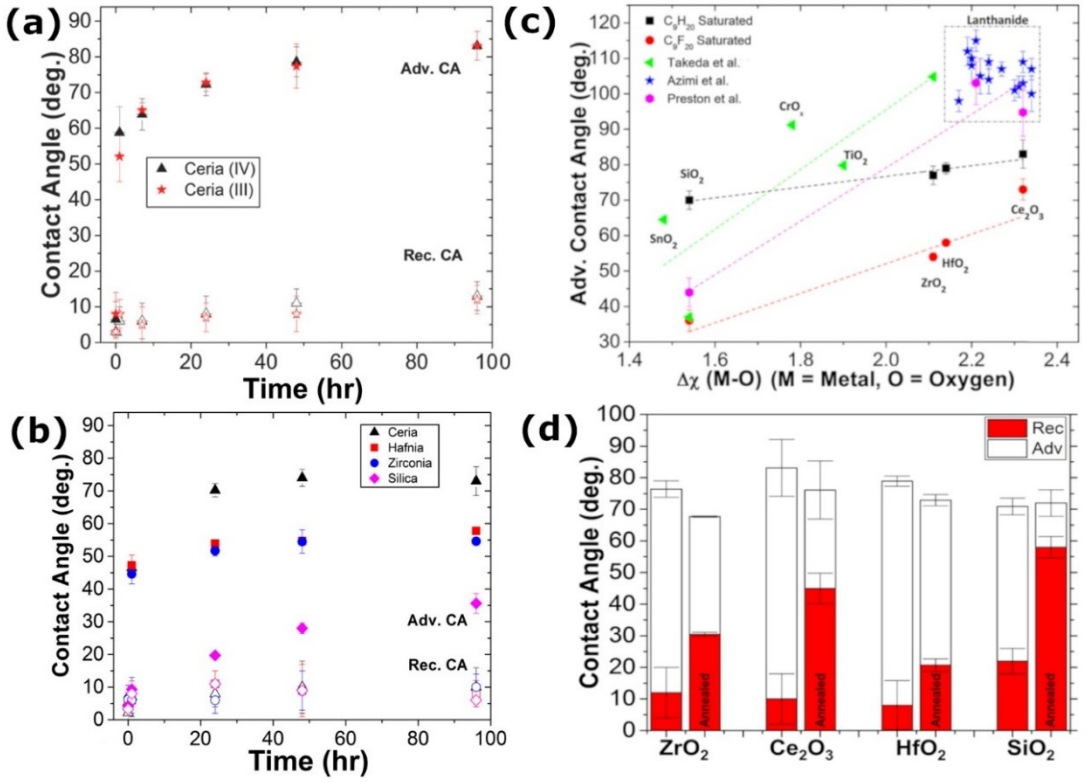

Figure 4 – Wettability and wetting to non-wetting/less-wetting transitions and surface carbon content in time from Lundy *et al.*[51]. (a) (solid symbols) Advancing contact angle (deg) and (empty symbols) receding contact angle versus time (hours) under laboratory air environment and **(b)** (solid symbols) Advancing contact angle (deg) and (empty symbols) receding contact angle versus time (hours) under perfluorononane C_9F_{20} environment. **(c)** Saturated advancing contact angle (deg) versus electronegativity difference between the element studied and the element studied as: $\Delta\chi$(M-O) under (black squares) a nonane C_9H_{20} and (red circles) perfluorononane C_9F_{20} environments from Lundy *et al.*[51], as well as results from the work of (green left-triangles) Takeda *et al.*[18], (blue stars) Azimi *et al.*[13], and (pink hexagons) Preston *et al.*[16]. **(d)** (white shaded) Advancing and (red shaded) receding contact angles in saturation conditions for zirconia ZrO_2, ceria (III) Ce_2O_3, hafnia HfO_2, and silica SiO_2, before and after annealing at 900° and ambient exposure from Lundy *et al.*[51]. Copyright 2017 American Chemical Society.

More recently, Oh *et al.* carried out a systematic study of wettability transition on several surfaces including metals such as silver and copper, other rare earth oxides including niobium pentoxide (Nb_2O_5) and ytterbia (ytterbium oxide Yb_2O_3) [19]. The use of ceria and silica allowed for the direct quantitative comparison on the atmosphere mediated wettability transition with earlier works in the literature [13, 16, 51-53]. Wettability characterisation through water droplet snapshots on ceria and copper surfaces after oxygen plasma cleaning function of the surface exposure to the ambient are shown in **Fig. 5a** and **Fig. 5b**, respectively. In addition to quantitatively addressing the wetting to non-wetting transition taking place from an intrinsically hydrophilic oxygen plasma clean surface to a HCs/VOCs masked one (**Fig. 5c**), Oh *et al.* additionally studied the different wettability of the same surfaces after cleaning with organic solvents in an ultrasonic bath function of ambient exposure (**Fig. 5d**). Organic solvents such as ethanol, acetone and isopropanol can wash off the physisorbed VOCs and HCs, but are unlikely to completely remove the VOCs or HCs chemically adsorbed onto the surface through strong molecular bonds [19, 54-56]. Hence, the surface wettability before and after

organic solvent cleaning remains within a similar contact angle range as represented in **Fig. 5c**. In contrast, under plasma cleaning, sufficient energy is imparted to the oxygen atoms to excite both physisorbed and chemisorbed VOCs/HCs removing them from the surface. By doing so, the intrinsic hydrophilicity of the outermost layer, which is now free of hydrophobic VOCs/HCs, is exposed to the ambient yielding contact angles as low as 40°. As the ambient exposure time increases, so does the droplet contact angle with rises in the order of tens of degrees ensuing within a day. In the particular case of copper, contact angles as high as 100°, i.e., in the hydrophobic regime, are reported after 100 hours of exposure (**Fig. 5d**). Although the results **Fig. 5c**, **Fig. 5d** and **Fig. 5e** are represented using a normal-log representation, the linear increase in the advancing contact angle with exposure time[19] agrees well both qualitatively and quantitatively with the logarithmic asymptotic behaviours earlier reported in a normal-normal representation in **Fig. 3c** and **Fig. 3d** as well as in **Fig. 4b** [16, 51]. Moreover, the ubiquitousness and universality of the transitions reported here, although the atmosphere-mediated superhydrophobicity was earlier demonstrated in China[20], USA[20], and Japan[35], were further demonstrated at Kyushu University in Japan, results which are included in **Fig. 5e**. When comparing **Fig. 5d** and **Fig. 5e**, *i.e.*, experimental work carried out at the University of Illinois at Urbana-Champaign (USA) that at Kyushu University (Japan), a rather good qualitative agreement is found when looking at the increase in the advancing contact angle function of laboratory ambient exposure for the same surfaces studied.

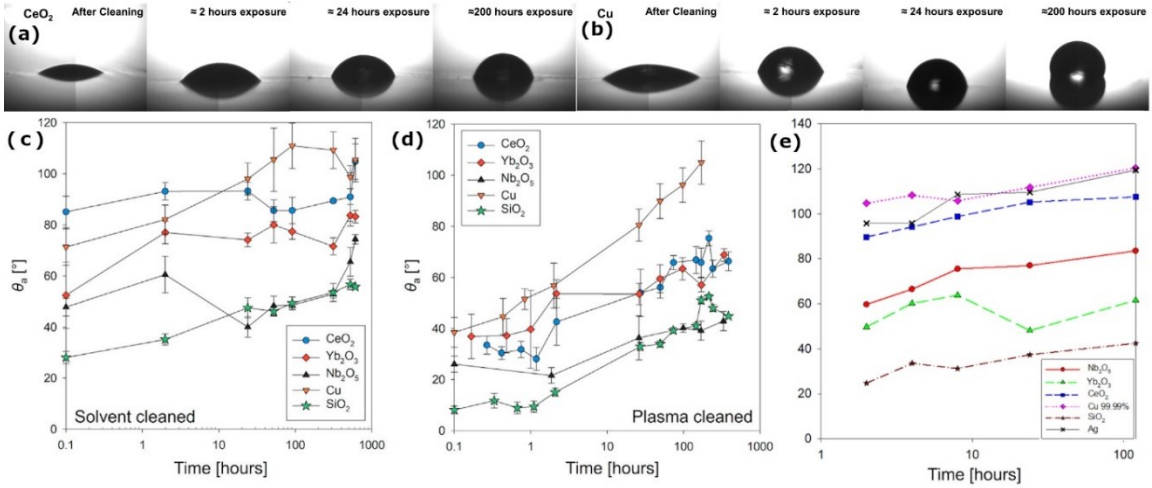

Figure 5 – Wetting to non-wetting/less-wetting transitions in time from Oh et *al.*[19]. Droplet profile versus exposure time (hours) for **(a)** ceria CeO_2 and **(b)** copper Cu. Advancing contact angle (deg) versus exposure time (hours) **(c)** after solvent cleaning and **(d)** after oxygen plasma cleaning at the University of Illinois at Urbana-Champaign (UIUC) in USA for (blue circles) ceria, (red diamonds) ytterbia, (black upward-triangles) niobium pentoxide, (orange downwards-triangles) copper, and (green stars) silica. **(e)** Advancing contact angle (deg) versus exposure time (hours) after oxygen plasma cleaning at Kyushu University in Japan for (red circles) niobium pentoxide, (green upwards-triangles) ytterbia, (blue squares) ceria, (pink diamonds) copper, (brown stars) silica, and (black crosses) silver. Copyright 2022 Elsevier Inc.

After having reviewed the main works providing account for the wettability and for the wetting to non-wetting/less-wetting transitions reported on smooth solid surfaces in **Fig. 2** to **Fig. 5,** the different kinetics of VOCs/HCs adsorption associated to the different contact angle change dynamics and the atmosphere mediated wetting transitions in time are highlighted. Next, a figure of merit reporting a summary of the state-of-the-art contact angle function of the carbon content %C owed to VOCs/HCs adsorption is provided.

Figure of merit

As reviewed above, the presence of carbon from volatile organic compounds (VOCs) masking the intrinsic wettability of solid surfaces has been reported on: aluminium [17], stainless steel [50], titanium oxide [18], chromium oxide [18], zirconium oxide [18, 51], holmia [16], ceria(III) [51], ceria(IV) [16, 51], gold [16], silica [16], copper [19], niobium pentoxide (Nb_2O_5) [19], ytterbia or ytterbium oxide (Yb_2O_3) [19], and hafnium oxide (HfO_2) [51], amongst others. A figure-of-merit summarising most of the published research to date on the wettability (contact angle) as a function of carbon surface atomic percent (%C) for surfaces exposed to ambient laboratory conditions and to saturated VOCs/HCs environments is shown in **Fig. 6a** and **Fig. 6b** respectively.

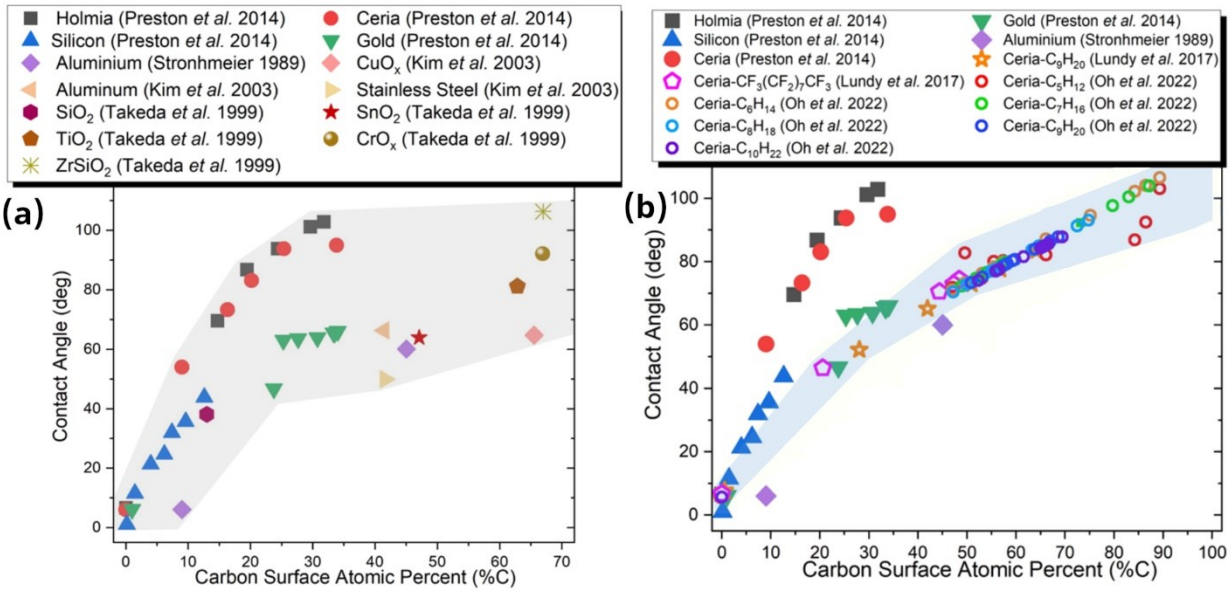

Figure 6 - Figure-of-merit representing contact angle θ (deg) vs. carbon surface atomic percent (%C). (a) Smooth surfaces exposed to laboratory environment in shaded grey and solid symbols: ■ holmia [16], ▼ gold [16], ▲ SiO_2 [16], ● ceria [16], ♦ aluminium [17], ♦ CuO_x [50], ◀ aluminium [50], ▶ stainless steel [21], ⬢ SiO_2 [18], ★ SnO_2 [18], ⬟ TiO_2 [18], ● CrO_x [18], and ✳ $ZrSiO_2$ [18]. Note that most of the data reported in **Fig. 6a** was earlier included in the Supplementary Information in Preston *et al.* [16]. Grey shaded area in Fig. 6a is for illustration purposes and self-contain all the reported experimental data under ambient laboratory exposure conditions. **(b)** Smooth surfaces exposed to laboratory environment from **Fig. 6a** in solid symbols along with smooth ceria exposed to different saturated VOCs environments in shaded blue and open symbols: ⬠ nonane C_9H_{20} [51], ☆ perfluorononane $CF_3(CF_2)_7CF_3$ [51], and ○ pentane C_5H_{12}, ○ hexane C_6H_{14}, ○ heptane C_7H_{16}, ○ octane C_8H_{18}, ○ nonane C_9H_{20}, and ○ decane $C_{10}H_{22}$ [19]. Blue shaded area in **Fig. 6b** is for illustration purposes and self-contain all the reported experimental data under ambient laboratory exposure conditions while data from **Fig. 6a** is included for comparison.

While **Fig. 6a** provides a summary of the contact angle/wettability results for surfaces exposed to ambient laboratory conditions, **Fig. 6b** includes the same surfaces reported in **Fig. 6a** with the addition of smooth ceria exposed to different saturated VOCs/HCs environments (pentane C_5H_{12}, [19] hexane C_6H_{14}[19], heptane C_7H_{16}[19], octane C_8H_{18}[19], nonane C_9H_{20}[19, 51], decane $C_{10}H_{22}$ [19], and perfluorononane

$CF_3(CF_2)_7CF_3$ [51]). When looking into both figures, an obvious direct linear increase in the droplet contact angle with carbon content is noticed both for surfaces exposed to laboratory conditions in **Fig. 6a** as well as for surfaces exposed to VOCs/HCs saturated environments as highlighted by the shaded blue area in **Fig. 6b**.

On one hand, the wetting to non-wetting transitions on rare earth oxides such as ceria and holmia undergo a change in wettability from 10° to 70° for a 15% carbon content with final contact angles as high as 100° for a carbon content near 30% [16]. On the other hand, transition metals such as gold reach near 70° for a 35% carbon content while metalloids such as silica see an increases to nearly 50° for a 15% carbon content [16]. To this end, while rare earth oxides transition from wetting to non-wetting, metalloids and transition metals transition instead from wetting to less-wetting, i.e., a final contact angle < 90°. Likewise, despite the greater carbon content adsorbed onto other post-transition metals such as aluminium[50] and stainless steel [21] as well as post-transition metals oxides such as SnO_2 [21], these experience a wetting to less-wetting transition with final contact angles between 50° and 70°, i.e., < 90°. Transition metal oxides such as CrO_x [21], CuO_x [50], TiO_2 [21], and $ZrSiO_2$ [21] showed the greatest content of carbon on the surface and contact angles ranging from 60° to 110° for CuO_x and $ZrSiO_2$, respectively.

When looking at saturated VOCs/HCs environments, the wetting to non-wetting transitions function of ambient exposure are further demonstrated in **Fig. 6b**. When comparing the results in **Fig. 6a** and **Fig. 6b**, even though ceria is able to adsorb a greater content of carbon %C under saturated VOCs/HCs environments, the magnitude of the contact angles reported at saturation reach similar quantitative values. More specifically, an increase in the contact angle from nearly 10° to 100°/110° as the carbon content increases is noticed, which is in agreement with earlier observations for ceria exposed to ambient laboratory conditions [16]. When looking into the different saturated VOCs/HCs environments, a 90% carbon content was measured on ceria exposed to saturated medium-chain HCs such as pentane C_5H_{12}, hexane C_6H_{14}, and heptane C_7H_{16}, with final contact angles equal or above 90°. On the other hand, for ceria exposed to saturated longer-chain HCs such as octane C_8H_{18}, nonane C_9H_{20}, and decane $C_{10}H_{22}$, for an adsorbed carbon content not greater than 80%, the contact angles remain below 90°, i.e., a wetting to less-wetting transition. It is worth noting the remarkable quantitative agreement between ceria exposed to octane C_8H_{18} or nonane C_9H_{20} (Oh *et al.*) and ceria exposed to nonane C_9H_{20} (Lundy *et al.*) with contact angles near 70° and 40% to 50% carbon content. Moreover, it is worth highlighting the wider grey shaded region reported in **Fig. 6a** when compared to the narrower blue shaded region in **Fig. 6b**, which is presumably due to the wider range of surfaces, different adsorption kinetics as well as different surface-VOCs-liquid droplet interactions when compared to Ceria exposed to VOCs saturated conditions.

Although the figures of merit shown in **Fig. 6a** and **Fig. 6b** provide the relevant direct quantitative relationship between contact angles/wettability and carbon content/HCs adsorbed on the surface, they do not provide any further insights on the droplet-surface interaction such as pinning, lateral adhesion, and/or the mechanisms, kinetics and/or selectivity of VOCs/HCs adsorption taking place. Furthermore, it is also not possible to quantify the wettability function carbon content/HCs adsorbed of carbon-based materials such as suspended and supported graphene [57, 58], and graphite [57, 58], amongst others. Hence, further work is needed to explore and understand the adsorption mechanism along with the different VOCs-surface

interactions and their impact on wetting. To this end, mapping the carbon content versus time may provide the relevant and necessary insights to better understand the kinetics of VOCs/HCs adsorption.

Pinning and lateral adhesion

As volatile organic compounds (VOCs) adsorption modifies the physicochemical properties of the solid surface, both in terms of wettability as well as physical and chemical composition, adsorption also plays a fundamental role on liquid droplet pinning and adhesion. To this end, droplet contact line pinning or lateral adhesion can be considered as a metric to quantify the affinity that a liquid droplet may have for a surface. For a droplet on an inclined smooth surface, the seminal work of Furmidge [59] proposes a force balance where a *retention factor* or pinning force, F_{pin}, could be quantified by equalling it to the gravitational force pulling the droplet down, F_g. The *retention factor* or pinning force, F_{pin}, is in fact a function of both the advancing and receding contact angles, θ_a and θ_r, or contact angle hysteresis [60, 61], which in itself is a function of time, t, and/or the surface carbon content, %C. To date, only a handful of works [16, 19, 51] have reported on both the advancing and receding contact angles function of ambient exposure time, which are included in **Fig. 7**.

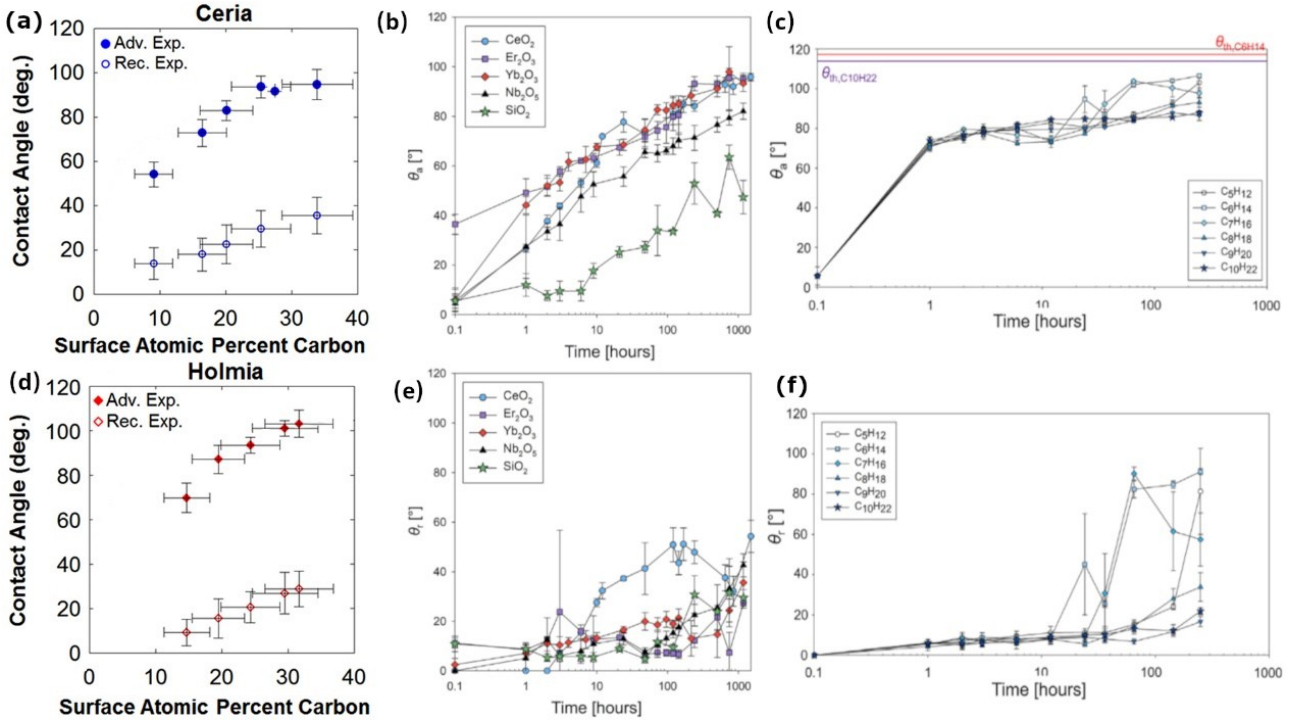

Figure 7 – Advancing and receding contact angle transition function of the surface carbon content %C and/or exposure time from Preston *et al.*[16] and Oh *et al.*[19] while that of Lundy *et al.*[51] was already represented in Fig. 4. (a) and **(d)** (solid symbols) Advancing contact angle, θ_a (deg), (empty symbols) receding contact angle, θ_r (deg), and (dashed lines) advancing model, versus carbon content %C for ceria and holmia respectively from Preston *et al.*[16]. Copyright 2014 American Institute of Physics. **(b)** (solid symbols) Advancing contact angle, θ_a (deg), and **(e)** (solid symbols) receding contact angle, θ_r (deg), versus time, t (hours), for different smooth rare earth oxides and rear earth oxides, metalloids oxide and transition metal oxides from Oh *et al.*[19]. Copyright 2022 Elsevier Inc. **(c)** Advancing contact angle, θ_a (deg), and **(f)** receding contact angle, θ_r (deg), versus time, t (hours), for ceria exposed to different VOCs/HCs saturated environments: ○ pentane C_5H_{12}, ○ hexane C_6H_{14}, ○ heptane C_7H_{16}, ○ octane C_8H_{18}, ○ nonane C_9H_{20} and ○ decane $C_{10}H_{22}$ from Oh *et al.*[19]. Copyright 2022 Elsevier Inc.

When looking at **Fig. 4a** and **Fig. 4c**, as well as **Fig. 7** above, an increase in the advancing contact angle θ_a in an asymptotic fashion ensues. On one hand, the contact angle increases rapidly at early stages of ambient exposure and/or carbon content %C reaching a constant plateau at later stages of exposure time. On the other hand, the receding contact angle θ_r undergoes a linear increase with either carbon content %C or

exposure time. From the abovementioned figures, the difference between the advancing and receding contact angles, θ_a and θ_r, or the contact angle hysteresis (θ_a - θ_r) as a function of either the carbon content %C or laboratory ambient exposure time, can be quantified. Fundamentally, for a droplet to start moving on a horizontal substrate, a force overcoming the pinning force or the surface hysteresis is required. **Equation 2** provides the necessary quantification of the pinning force, F_p, based on its advancing and receding contact angles, respectively, on the droplet base width w and equals D_b or $2R_b$, and on the constant $k = 1$, as proposed in Furmidge's seminal work [59] and widely implemented in several later works [49, 62-66]:

$$F_{pin} = kw\gamma_{\mathrm{lg}}(\cos\theta_r - \cos\theta_a) \tag{2}$$

Hence, by making use of the advancing and receding contact angles reported in **Fig. 4a**, **Fig. 4b**, and **Fig. 7**, and **Eq. 2**, the *retention factor* or pinning force function of ambient laboratory conditions exposure time ($F_{\mathrm{pin}}(t)$) and/or function of the carbon content (F_{pin}(%C)) for different substrates are quantified and represented in **Fig. 8** and **Fig. 9**. More in particular, **Fig. 8** shows both the contact angle hysteresis, CAH = θ_a - θ_r, and the estimated pinning force, F_{pin}, function of laboratory exposure time calculated from Oh *et al*. [19] and/or **Fig. 7** for different rare earth oxides, a transition metal oxide and a metalloid oxide after solvent and plasma cleaning.

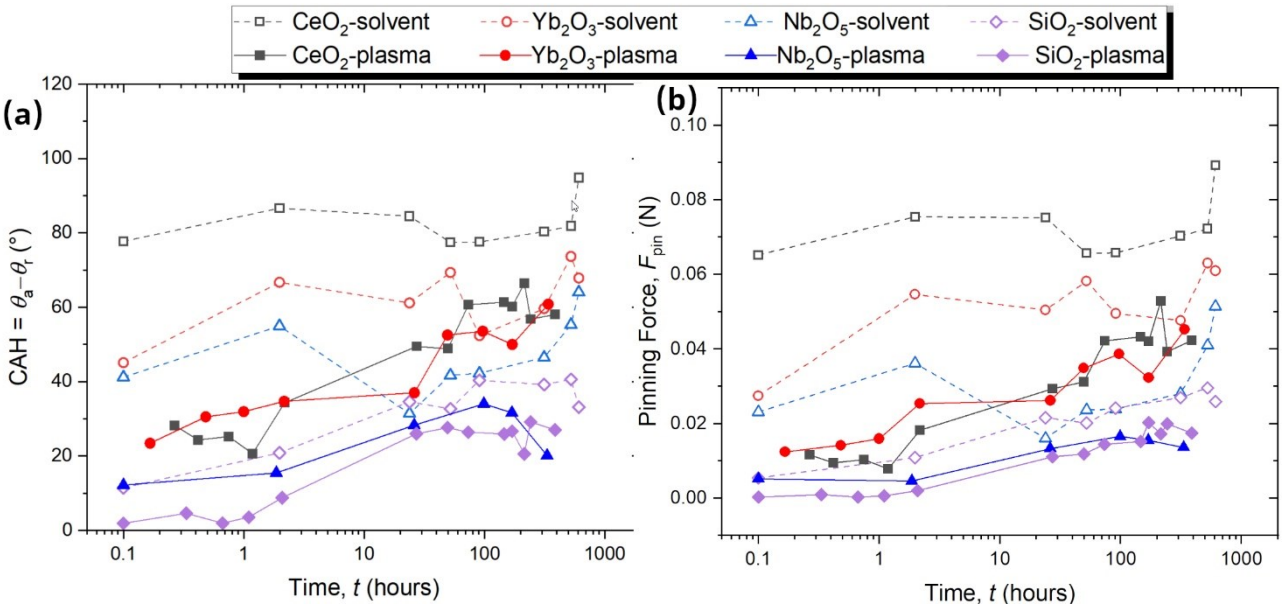

Figure 8 – Contact angle hysteresis and pinning force function of ambient laboratory exposure time calculated from Oh *et al.* [19] by making us of Fig. 7 and Eq. 2. (a) Contact angle hysteresis, CAH = θ_a - θ_r (deg), and **(b)** pinning force, F_{pin}, function of ambient laboratory exposure time, t (hours), for (squares) ceria, (circles) ytterbia, (up triangles) niobium oxide, and (diamonds) silicon oxide, after (empty symbols) solvent cleaning and (solid symbols) plasma cleaning.

From **Fig. 8** a similar trend on the reported CAH and F_{pin} function of ambient exposure time is reported. Indepdently of the nature of the surface, F_{pin} increases with ambient laboratory exposure time as expected from the F_{pin}-CAH relation established by **Eq. 2**. From **Fig. 8** it is evident that the CAH and F_{pin} values increase as surfaces are exposed to the ambient, though the magnitude of such increase depends on the nature of the solid surface as well as the cleaning procedure. CAH values reported can vary from nearly 0° to 100° with pinning

forces varying from nearly 0 N right after plasma cleaning in the case of SiO_2 to as high as 0.3 N in the case of ceria after solvent cleaning after long ambient laboratory exposure times.

More specifically, when looking into the CAH right after solvent cleaning, surfaces display a wide range of contact angle hysteresis. CAH for ytterbia and niobium oxide is similar as approximate 40° while ceria and silicon oxide show quite different CAH, as 80° for ceria and 10° for SiO_2. In case of the solvent cleaned surfaces, as these surfaces are exposed to ambient laboratory conditions after the cleaning, the CAH typically increases as reported in **Fig. 8a** due to mainly physisorption of VOCs/HCs. Although the magnitude of the advancing and receding contact angles vary depending on the nature of the materials (**Fig. 7**), after solvent cleaning all surfaces report a similar increase in the CAH between 20° to 30° within hundreds of hours from cleaning. On the other hand, after plasma cleaning, the surfaces display contact angle hysteresis between 0° and 30° within 1 hour from cleaning, which is considerably lower than the CAH reported after solvent cleaning. On these plasma cleaned surfaces, the increases in the CAH more evidently tells the nature of the surface. In the case of the ceria and ytterbia (two rare earth oxides), and silicon oxide (metalloid oxide), a CAH increase of approximately 20° to 30° is reported, whereas in the case of the niobium oxide (transition metal oxide) only a final increase of 10° is reported. While the increase in the surface CAH after both solvent and plasma cleaning are within the same order of magnitude, shown in **Fig. 8a**, it is important to note the lower magnitude of the final CAH for those surfaces cleaned with plasma. A decrease in the CAH of 5° to 10° is reported for silicon oxide and ytterbia, while up to 40° lower CAH is established for ceria and niobium oxide surfaces, when comparing plasma cleaned to solvent cleaned surfaces at the same exposure time. The two to four-fold smaller CAH reported for ceria and niobium oxide surfaces should in turn offer lower pinning forces F_{pin} and ease the droplet mobility over the same surface.

When looking at the F_{pin} in **Fig. 8b**, similar qualitative trends are reported as in **Fig. 8a**. For all analysed cases, an increase in the pinning force F_{pin} with exposure time is reported indepdently of the cleaning procedure either using solvent or plasma. The initial magnitude of the pinning force as well as the increase in the pinning force in time, are both function of the nature of the material as well as the cleaning procedure. Right after solvent cleaning the pinning force ranges between 0.07 N for ytterbia and niobium oxide to 0.2 N for ceria, while 0.02 N is reported on silicon oxide. Whereas right after plasma cleaning all initial pinning forces for all studied surfaces are found below 0.05 N. As the surfaces are exposed to the ambient, solvent cleaning surfaces reach values between 0.1 and 0.3 N while pinning forces below 0.15 N are obtained after plasma cleaning.

It is then clear that both the CAH and the droplet pinning force are function of the laboratory ambient exposure time and more importantly of the cleaning method. When comparing the different pinning forces function of the cleaning procedure, 2.2 to 5.6 times lower pinning forces are quantified on surfaces cleaned with plasma when compared to those cleaned with a solvent. Silicon oxide and ceria show the greater differences on the initial pinning force whereas that of ytterbia is only two-fold. As the surfaces are exposed to laboratory conditions, the CAH increases and so does the pinning force while the ratio of solvent cleaning to plasma cleaning pinning force decreases. Nonetheless, up to 1.5 to 2.1 lower pinning forces are reported for silicon oxide and niobium oxide, respectively while ytterbia only sees a 5% decrease after 300 hours of exposure.

From **Fig. 6b**, **Fig. 7e** and **Fig. 7f** it is also clear that the wettability as well as the advancing and receding contact angles for ceria differ as the same surface is exposed to different saturated VOCs/HCs environments such as pentane C_5H_{12}, hexane C_6H_{14}, heptane C_7H_{16}, octane C_8H_{18}, nonane C_9H_{20} and decane $C_{10}H_{22}$ [19]. It is worth noting that the receding contact angle undergoes a greater increase at the later stages of exposure to pentane C_5H_{12}, hexane C_6H_{14} and heptane C_7H_{16}, as shown in **Fig. 7f**. Such increase in the receding contact angle, in turn results in the CAH decrease and hence lower pinning forces when subjected to long exposure times. The contact angle hysteresis, CAH = θ_a - θ_r, and the calculated pinning force, F_{pin}, for ceria exposed to different saturated VOCs/HCs environments from Oh et al. [19] are represented in **Fig. 9**.

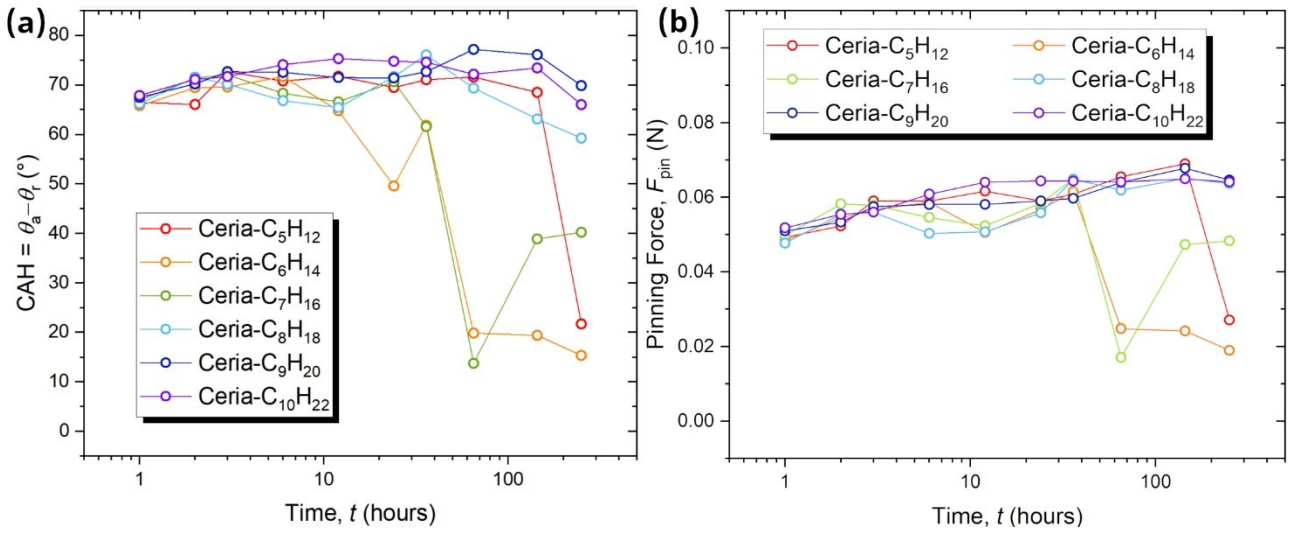

Figure 9 – Contact angle hysteresis and pinning force function of saturated VOCs/HCs environment exposure time calculated from Oh *et al.*[19] by making use of Fig. 7 and Eq. 2. (a) Contact angle hysteresis, CAH = θ_a - θ_r (deg), and **(b)** pinning force, F_{pin}, function of ambient laboratory exposure time, t (hours), for ceria exposed to saturated (red circles) pentane C_5H_{12}, (orange circles) hexane C_6H_{14}, (green circles) heptane C_7H_{16}, (light blue circles) octane C_8H_{18}, (dark blue circles) nonane C_9H_{20}, and (purple circles) decane $C_{10}H_{22}$.

Looking at **Fig. 9a**, an initial contact angle hysteresis as high as 65° is reported independently of the saturated VOCs/HCs environment. As the surfaces are exposed to the different saturated environments, two clear trends are observed. On one hand, in the case of long HC chains such as octane C_8H_{18}, nonane C_9H_{20}, and decane $C_{10}H_{22}$, a slight increase on the contact angle hysteresis or a plateau is reported with all values ranging between 65° and 75° at any exposure time. On the other hand, for medium HC chains such as pentane C_5H_{12}, hexane C_6H_{14} and heptane C_7H_{16}, a decrease in the contact angle hysteresis occurs after a day of exposure under hexane C_6H_{14} and heptane C_7H_{16} and after several days, i.e., 100 hours, under pentane C_5H_{12}. Equivalently, the pinning forces reported in **Fig. 9b** also undergo similar trends with a plateau or slight increase in the pinning force under long HC chains environment exposure (octane C_8H_{18}, nonane C_9H_{20}, and decane $C_{10}H_{22}$) with values oscillating between 0.15 and 0.25 N. Whereas pinning forces below 0.1 N are reported for medium HC chains (pentane C_5H_{12}, hexane C_6H_{14} and heptane C_7H_{16}) after long exposure times. The decrease on both the CAH and the pinning force of up to 2- fold lower for ceria surfaces exposed to saturated medium HC environments as (C_5H_{12}, C_6H_{14} and C_7H_{16}) highlighted in **Fig. 9b** needs special mention and may find importance in applications where the mobility of a droplet must be finely controlled.

The above results and discussion indicate that more studies and research efforts on the effect of our surrounding environment on the physicochemical properties changes of solid surfaces is of much need. This includes the better understanding and quantification of the different interfacial tensions γ_{sl} and γ_{sg} governing the wetting to non-wetting transitions as well as the dynamic changes in contact angle hysteresis, pinning and adhesion function of the environment composition as well as the exposure time. The change in the γ_{sl} as a function of ambient exposure time, i.e., VOCs/HCs adsorption, can be further quantified via the application of a novel meniscus based direct measurement of the solid-liquid interfacial energy [45]. The work of adhesion [63] and/or the static and dynamic friction factors [66, 67] are also some of the other metrics that deserve further consideration, and experiments via tensiometer and droplet force measurements are suggested.

Adsorption models

As clearly introduced above, the chemical composition of the outermost layer of solid surfaces changes in time as volatile organic compounds(VOCs)/HCs adsorb onto these surfaces when they are exposed to the ambient environment. In order to model the change in contact angle as a function of the VOCs/HCs adsorption or carbon content, Preston *et al.* and Lundy *et al.* adopted the Cassie-Baxter equation [68] assuming chemical heterogeneities instead of physical heterogeneities assumed originally by the Cassie-Baxter equation [16, 51]. In other words, the equilibrium contact angle, θ_0, is estimated by assuming adsorbed VOCs/HCs as defined hydrophobic regions while non-covered areas remain hydrophilic following **Eq. 3** [16, 69]:

$$\cos\theta_0 = \varphi\cos\theta_{0,\mathrm{HC}} + (1-\varphi)\cos\theta_{0,\mathrm{clean}} \qquad (3)$$

where φ is the apparent surface coverage, $\theta_{0,\mathrm{HC}}$ is the equilibrium contact angle on the smooth surface exposed to the ambient for prolonged times (fully covered/saturated with VOCs: $\varphi = 1$), and $\theta_{0,\mathrm{clean}}$ is the equilibrium contact angle on the smooth cleaned surface (absence of VOCs: $\varphi = 0$). VOCs surface coverage φ can then be estimated from the carbon atomic composition on the surface through surface chemical characterization such as XPS [16] or EDS [35]. **Figure 10** includes the different efforts on the direct relationship between apparent surface coverage φ and wettability or contact angle function of carbon content or exposure time.

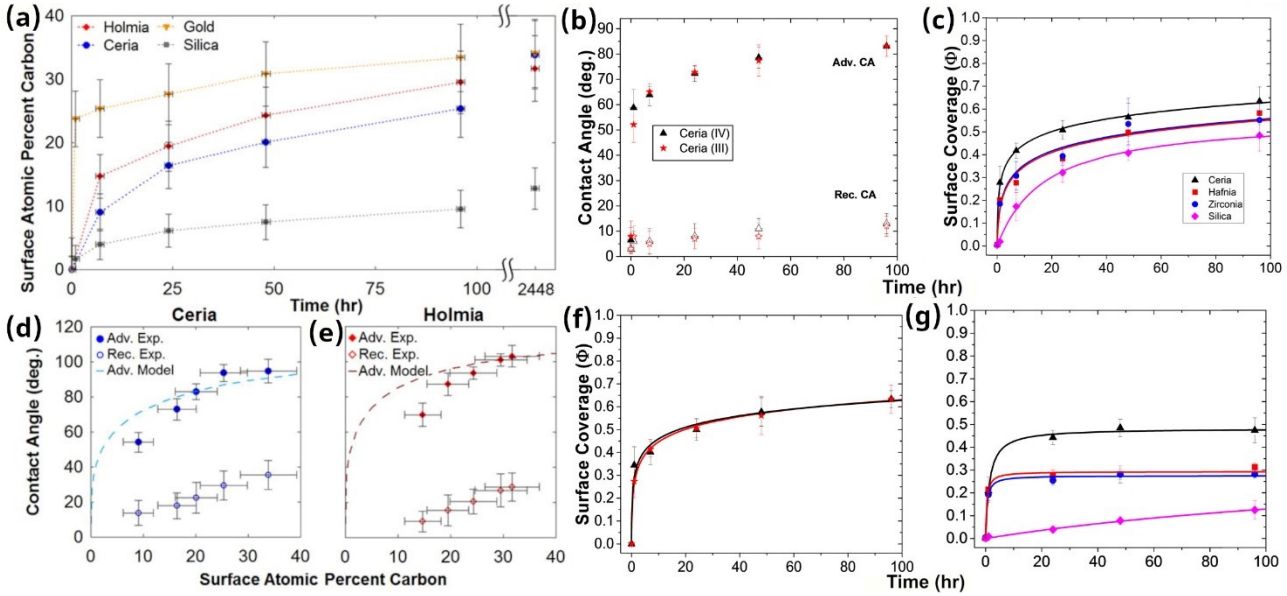

Figure 10 – Models on the surface atomic carbon content %C, contact angle or surface coverage φ as a function of time. (a) Surface atomic carbon content %C quantified via XPS function of time (hours) used to estimate the contact angle function of surface atomic carbon content (%C) in **(d)** (blue circles) ceria and **(e)** (red circles) holmia from Preston *et al.* [16]. Copyright 2014 American Institute of Physics. **(b)** Advancing and receding contact angles (deg) function of time (hours) used to estimate **(f)** the surface coverage φ as a function of time (hours) for (red stars) ceria (III) Ce_2O_3 and (black upwards-triangles) ceria (IV) CeO_2 under laboratory air environment from Lundy *et al.* [51]. Experimental and estimated surface coverage φ as a function of time (hours) for (black triangles) ceria (IV) CeO_2, (red squares) hafnia HfO_2, (blue circles) ZrO_2, and (pink diamonds) SiO_2 under **(c)** nonane C_9H_{20} and **(g)** perfluorononane C_9F_{20} environments from Lundy *et al.*[51]. Copyright 2017 American Chemical Society.

From **Eq. 3** and the surface atomic carbon content %C in time (**Fig. 10a**), a theoretical prediction of the contact angle can be drawn for both ceria and holmia as established in **Fig. 10d** and **Fig. 10e**, respectively[16]. A remarkable qualitative asymptotic agreement on the change in contact angle function of

carbon content, *i.e.*, on the wetting to non-wetting transition, is then established for both rare earth oxides, which demonstrates the validity of the model proposed. Moreover, a rather good quantitative agreement is also found, within the error bounds of the measurements, for medium and high surface carbon content %C or apparent surface coverage $\varphi > 0.15$, i.e., for carbon content equal to or above 15%. This highlights that the model works appropriately as the surface becomes saturated with VOCs/HCs and the apparent contact angle approaches that on the saturated surface, i.e., $\theta_0 = \theta_{0,HC}$, which is the case for long exposure times. However, it fails to provide an accurate estimation of the contact angle for low exposure times and/or for low surface carbon content %C or low apparent surface coverage φ; and/or to capture quantitatively and qualitatively the receding contact angle trends reported in both **Fig. 10d** and **Fig. 10e**.

Thereafter, Lundy *et al.* applied a reversed approach where the surface carbon content %C or apparent surface coverage φ reported in **Fig. 10f** was actually inferred from the contact angle measurements reported in **Fig. 4a** or **Fig. 10b** instead [51]. This was also carried out for ceria under nonane C_9H_{20} and perfluorononane C_9F_{20} represented **Fig. 10c** and **Fig. 10g**. In fact, such reversed approach to estimate the surface coverage φ inferring the surface carbon content %C provides actually more flexibility and room for the fitting of the actual data to the model instead of the other way round as in Preston *et al.* [16]. As such a better and more accurate qualitative and quantitative agreement are reported in **Fig. 10c**, **Fig. 10f**, and **Fig. 10g**, when compared to **Fig. 10d** and **Fig. 10e**. As a common feature and as reported within this work, both the contact angle and the surface coverage increase asymptotically towards a saturation value. In addition, for all cases the shape of these curves as well as the final values are functions of both the nature of the solid surface as well as the composition of the environment. When looking into different environments, the lower quantitative surface coverage φ in the presence of perfluorononane C_9F_{20} when compared to nonane C_9H_{20} can be presumably attributed to the more hydrophobic nature of fluorine termination groups within the perfluorononane C_9F_{20}, which yields greater $\theta_{0,HC}$ for lower surface coverage φ evident when comparing **Fig. 10c** to **Fig. 10g**. Here the intermediate and final value differences are not negligible with differences in the values ranging from 10% for ceria, to 80% for hafnia and to 235% for silica after 96 hours of exposure.

In order to quantify the surface coverage φ reported in **Fig. 10c**, **Fig. 10f**, and **Fig. 10g**, the following modified equation, **Eq. 4**, based on a molecular scale chemical heterogeneities was utilised [70]:

$$\varphi = \frac{(1+\cos\theta_0)^2 - (1+\cos\theta_{0,\text{clean}})^2}{(1+\cos\theta_{0,\text{HC}})^2 - (1+\cos\theta_{0,\text{clean}})^2} \quad (4)$$

where φ is the apparent surface coverage, θ_0 is the equilibrium contact angle on the surface, $\theta_{0,HC}$ is the equilibrium contact angle on the smooth surface exposed to the ambient for prolonged times (without assuming $\varphi = 1$ for fully VOCs coverage as opposed to **Eq. 3**), and $\theta_{0,clean}$ is the equilibrium contact angle on the smooth cleaned surface (absence of VOCs and $\varphi = 0$). Nonetheless, both **Eq. 3** and **Eq. 4** fail to capture the kinetics and selectivity of VOCs/HCs adsorption as well as the effect of substrate nature and ambient composition on the wetting to non-wetting transition dynamics. To counteract this drawback Lundy *et al.* proposed an empirical relation to fit their data based on the Elovich fit following both the Israelachvili model [70] and the Cassie-Baxter model [68]. A remarkable agreement and regression coefficients equal to or above 0.98 were obtained. While the above model provides an excellent fitting to the surface coverage φ estimated from contact

angle experimental measurements, the utilisation of similar models to validate the actual data of surface carbon content %C yields less accuracy at earlier adsorption times or at low surface carbon content. Hence, other adsorption models such as the pseudo-first order[71], and/or the pseudo-second order rate laws[20, 72, 73], amongst others[73-75] may be considered.

Of equal importance is the need to understand the specific species adsorbing onto solid surfaces, i.e., selectivity, and/or the type of adsorption mechanism either as physisorption or chemisorption. To this end, some studies have proposed the use of time-of-flight secondary ion mass spectroscopy (ToF-SIMS) aiming to elucidate the nature of the adsorbed species, though to date no quantification can be achieved through this technique [17, 19, 20]. Short carbon chains of VOCs such as C_3H_5, C_3H_7, C_4H_7 and C_4H_9 were identified under both hexane C_6H_{14} and nonane C_9H_{20} saturated environments [19]. Exposure to lighter hydrocarbons such as hexane C_6H_{14} yields higher counts of C_xH_y-positive secondary ions when compared to heavier or larger hydrocarbon chains such as nonane C_9H_{20}. Further, in the work of Oh *et al.*, depth ToF-SIMS profiles of ceria exposed to hexane C_6H_{14} showed the presence of C, H, and C + H ion, which counts intensity decreased with the number of layers depth [19]. Similar findings and presence of short/medium chain HCs in an aliphatic/straight chain such as $C_2H_3^+$, $C_2H_5^+$, CH_3O^+, $C_3H_3^+$, $C_3H_5^+$, $C_3H_7^+$, $C_4H_7^+$, $C_3H_9^+$, CH^-, O^-, OH^-, OH_3^-, $O_2H_3^-$, C_3H^- and CNO^-, were found adsorbed onto copper oxide in the works of Yan *et al.*[20, 76].

Summary and Perspective

Summary

The wetting to non-wetting (or to less-wetting) transitions on *bare* solid surfaces exposed to laboratory ambient conditions or other environments (outdoor) in the presence of volatile organic compounds (VOCs) have been summarised and reported. Although elucidated five decades ago and subsequently considered a nuisance by the scientific community, it is only recently that more rigorous efforts on shedding further light on this phenomenon have been undertaken. Past work has shown that the wetting to non-wetting transition as well as the surface carbon content %C are both functions of the nature of solid surface as well as the ambient VOC composition. Rare earth oxides such as ceria, holmia and hafnia exposed to ambient laboratory conditions are able to display non-wetting behaviour with contact angles above 90° in a matter of days of laboratory ambient exposure. These REOs have been reported to induce dropwise condensation behaviour of interest to heat transfer applications [13]. Conversely, transition metals such as gold, aluminium and stainless steel are able to adsorb larger quantities of VOCs than REOs while the maximum contact angles reported were near but below 90°, i.e., in this wetting regime, except for Cu which has an advancing contact angle near 100°, although dropwise condensation does not ensue in this latter [19]. While in the case of gold, even though water droplet contact angles reported were well below 90°, dropwise condensation ensued on such VOC coated surfaces [12]. Other metalloids such as silicon oxide adsorbs less carbon content and the final contact angles are below 50°. Such transitions and final wetting behaviours under laboratory conditions have been demonstrated in different geographical regions such as the USA, Japan, China and Ireland, amongst others, which demonstrates the ubiquitousness of VOCs and their adsorption onto solid surfaces.

We developed a figure-of-merit which includes the majority of published research work to date. Quantification of the contact angle as a function of the surface carbon content %C for surfaces exposed to ambient laboratory conditions and for those under different VOCs/HCs saturated environments is further reported and can be used as a guideline for selecting substrate materials based on the desired wettability for the specific application. To note is the similar final wetting behaviour reported in the case of some various surfaces and/or different environmental conditions. This behaviour suggests that when designing the application, other substrate properties such as thermal conductivity, heat capacity, elasticity, plasticity, availability as well as economic factors, need to be considered rather than wettability alone.

Since the change in the physicochemical properties of the surface brings changes to both the advancing and receding contact angles, which is directly linked to the contact angle hysteresis and to some extent to contact line pinning and lateral adhesion, the relevant estimation of the pinning force F_{pin} as a function of ambient exposure is established here. Lower pinning forces ensue on oxygen plasma cleaned surfaces exposed to ambient laboratory conditions when compared to those cleaned with organic solvents, which result in higher mobility droplets on the former. More importantly, the exposure to a saturated environment of medium length hydrocarbons i.e., pentane C_5H_{12}, hexane C_6H_{14}, and heptane C_7H_{16}, yielded a decrease in both the contact angle hysteresis and pinning forces, which can empower the design of low pinning surfaces.

Lastly, the different efforts focused on understanding the classification of this phenomenon either as physisorption and/or chemisorption have been introduced and discussed. Within these, studies looking at the

dynamics, kinetics, and selectivity of VOCs adsorption, as well as on the nature of the individual species adsorbed, have been analysed. All of these dynamic phenomena are shown to be functions of the solid surface as well as the composition of the surrounding environment, further motivating additional work.

Based on the past literature, there is an urgent need to develop a clear understanding of the fundamental and basic science mechanisms governing VOC adsorption since these mechanisms ultimately govern the wettability of otherwise intrinsically hydrophilic solid surfaces. Future perspectives and suggestions regarding research efforts to focus on as a scientific community are provided next.

Perspectives

It is of utmost importance from the fundamental science point of view to clearly and accurately understand the effects of our surrounding atmosphere on the change in the physicochemical properties of solid surfaces governing droplet wetting. This is important because control and tuning of the solid surface outermost layer composition via ambient exposure governs the liquid-surface, which can be tailored to the specific application including micro-fluidics, drag reduction and/or phase-change, amongst others. Moreover, the passive adsorption of volatile organic compounds (VOCs) ever present in the environment open the potential for self-healing capabilities, which is of great importance for the design of continuous, robust and durable processes and applications [19, 20, 35]. Besides playing a role on wettability [19], VOCs adsorption has also been hence reported to influence boiling [77], condensation [52, 76, 78], droplet evaporation [79], membrane distillation [80], opto-electronical properties [81], surface chemical analysis [33], and/or oil-water separation [82], and catalysis [83, 84], amongst others. In addition, besides playing a role on applications involving liquids and solid surfaces, VOC adsorption governs the emissivity and colour displayed in diamond-like carbon films [85, 86]. While it remains unclear whether these VOCs also contribute to the high non-wetting behaviour observed on carbon based materials such as suspended [58] and supported graphene [57, 58],

Differences in the mechanisms proposed and timescales estimated for the reported wetting to non-wetting transition dynamics call for further scientific investigation. These mechanisms are functions of the surface structure as well as substrate material. Hence, they require further efforts from the scientific community at the fundamental level to be able to scale the appropriate strategy to real applications such as boiling [87] and condensation [13] of smooth surfaces where VOCs have been found to play a major role when compared to bare pristine hydrophilic surface. Different classical interfacial measurement techniques and methodologies such as the Zisman [88], Fowkes [43], and Owens, Wendt, Rabel and Kaelble work [89-91] methods, can eventually be adopted to provide further insights regarding the change in different interfacial solid-gas and solid-liquid interfacial tensions as well as their polar and non-polar nature as a consequence of ambient exposure in time. In addition, recently developed techniques used to quantify the solid-liquid interfacial energy such as the direct measurement of the direct solid liquid interfacial energy via a meniscus technique [45] and/or via the static and advancing contact angle [92], can also provide relevant insights about how the physicochemical properties of the outermost layer changes as a consequence of exposure to ambient conditions in the presence of VOCs.

More importantly, on an intrinsically hydrophilic structured solid surface, the transition from super-wetting/superhydrophilic to super-non-wetting/superhydrophobic have been reported to ensue on nanowire

films [93], copper (Cu) foams [94], and hierarchical CuO surfaces [95]. Immediately after fabrication, CuO surfaces display hydrophilicity with contact angles ≤ 10º [93, 95]. As these surfaces are exposed to ambient conditions, the wettability transitions from wetting to non-wetting, which has been recently coined atmosphere-mediated superhydrophobicity [20]. Water droplet contact angles as high as 156º have been reported on CuO nanowire films within 7 hours of exposure [93]; ≈136º on Cu foams after several days of exposure [94]; > 150º on hierarchical CuO structures after 15 days of exposure [95]; ~160º on hierarchical CuO thermally grown structures enabling the occurrence of dropwise condensation [20]. From these results, the various final contact angles (ranging from 136º to 156º) as well as adsorption time-scales (from hours to weeks) reported, highlight the diverse wetting to non-wetting transition dynamics. In addition, several mechanisms have been proposed as responsible for such transitions, which needs further clarification [94, 95].

Developing design strategies to be able to store and keep solid surfaces free of VOCs and hydrocarbons is of paramount importance when surface cleanliness is warranted. For example, the loss of wicking affects and hinders the boiling heat transfer performance and capillary pumping as a consequence of VOCs adsorption due to the loss in superhydrophilicity [77, 96, 97]. Since both superhydrophilicity and superhydrophobicity are within the top 10 emerging technologies in chemistry in 2021 as highlighted by the International Union of Pure and Applied Chemistry (IUPAC) [98], careful consideration of the strategies used to expose (or prevent exposure of) smooth or structured surfaces to the VOC-leaden ambient must be undertaken. Moreover, whether these VOCs are useful to corrosion protection is also a topic which needs to be addressed. A recent strategy developed to prevent the adsorption of VOCs on surfaces of interest involves the use of VOCs free structured surfaces where VOCs have more affinity to these structures when compared to the stored surface [99]. Other approaches have used pressurized containment with a pure gas to keep VOCs out of the sample environment, with good success [100]. Immersion in water is another strategy that can keep these surfaces from adsorbing VOCs. Conversely, atmosphere mediated superhydrophobicity via VOCs adsorption has been exploited and realised after the fabrication of structured surfaces via thermal oxidation [20], wet etching, aluminium [101], copper laser texturing [97], or lithography followed by ceria film deposition and fluorosilane treatment [102].

The dynamics of VOC adsorption is such that the total amount of VOCs adsorbed is limited and no more VOCs are adsorbed after certain amount of time. This final adsorption state governs the water droplet contact angle on the surface and hence the heat transfer [103]. In order to counteract this, on one hand, surface modification by making use of functionalised activated carbon with high surface area [104] has been demonstrated as a competitive VOCs adsorbent with increased VOC selectivity. The more affinity of activated carbon [104] and polyvinylidene fluoride (support) single walled carbon nanohorns [105] to VOCs rather than to water also anticipates the hindering of blister occurrence, which could eventually leading to coating delamination [106]. Zeolites, which offer a wide range of chemical functional terminations, could be used to target the adsorption of specific VOCs [34, 107, 108]. Also woods and polyurethane foam surfaces have also found to contribute to the reduction, i.e., adsorption, of phthalates VOCs when compared to glass[109].

Hence, due to the wide range of materials, surface structures, mechanisms, time-scales and types of VOCs reported, a systematic and methodological study to address the effects of intrinsic wettability of the material (from metals and metal oxides to non-metals); surface length-scale (from smooth to micro- and to the nano-scale); nano-structure surface finish (from foams, to nano-needles and to nano-blades); on the kinetics

and selectivity of specific VOC adsorption coupled with the wetting transition as well as on the most suitable and relevant applications for ambient is of much need.

Acknowledgments

D.O., N.M., and Y.T., acknowledge the support from the International Institute for Carbon-Neutral Energy Research (WPI-I2CNER), sponsored by the Japanese Ministry of Education, Culture, Sports, Science and Technology. D.O. acknowledges The Royal Society and The Royal Society Research Grant 2020 Round 2 with reference code RGS/R2/202041. K.S. and D.O. further acknowledge the support received EC-RISE-ThermaSMART project from the European Union's Horizon 2020 research and innovation programme under the Marie Skłodowska-Curie grant agreement No. 778104; from the European Space Agency (ESA) through the project Convection and Interfacial Mass Exchange (EVAPORATION) with ESA Contract Number 4000129506/20/NL/PG; and from the UK Research and Innovation office (UKRI) Official Development Assistance (ODA) Impact and Development Grant No. GNCA_WT13397057. D.O., D.J.P., and K.S. acknowledge the support received from the 2022 University of Edinburgh–Rice University Strategic Collaboration Awards programme. N.M. acknowledges funding support from the Office of Naval Research (ONR) under grants No. N00014-16-1-2625 and N00014-21-1-2089. For the purpose of open access, the author has applied a Creative Commons Attribution (CC BY) license to any Author Accepted Manuscript version arising from this submission.

References

[1] Bonn D, Eggers J, Indekeu J, Meunier J, Rolley E. Wetting and spreading. Rev Mod Phys. 2009;81:739-805.
[2] Si Y, Yu C, Dong Z, Jiang L. Wetting and spreading: Fundamental theories to cutting-edge applications. Current Opinion in Colloid & Interface Science. 2018;36:10-9.
[3] Gambaryan-Roisman T, Starov V. Editorial overview: Recent progress in studies of complex wetting and spreading phenomena. Current Opinion in Colloid & Interface Science. 2021;55:101486.
[4] de Gennes PG. Wetting: statics and dynamics. Rev Mod Phys. 1985;57:827-63.
[5] de Gennes PG, Brochard-Wyart F, Quere D. Capillarity and Wetting Phenomena: Drops, Bubbles, Pearls, Waves: Springer New York; 2013.
[6] Wang Z, Orejon D, Takata Y, Sefiane K. Wetting and evaporation of multicomponent droplets. Physics Reports. 2022;960:1-37.
[7] Zhang Y, Guo M, Seveno D, De Coninck J. Dynamic wetting of various liquids: Theoretical models, experiments, simulations and applications. Advances in Colloid and Interface Science. 2023;313:102861.
[8] Young T. III. An essay on the cohesion of fluids. Philosophical Transactions of the Royal Society of London. 1805;95:65-87.
[9] Dupré MA. Theories Mecanique de la Chaleur. Paris1869.
[10] Schrader ME. Young-Dupre Revisited. Langmuir. 1995;11:3585-9.
[11] Erb RA. Wettability of Metals under Continuous Condensing Conditions. J Phys Chem. 1965;69:1306-9.
[12] Erb RA. Dropwise condensation on gold. Gold Bulletin. 1973;6:2-6.
[13] Azimi G, Dhiman R, Kwon H-M, Paxson AT, Varanasi KK. Hydrophobicity of rare-earth oxide ceramics. Nature Materials. 2013;12:315.
[14] Li Z, Wang Y, Kozbial A, Shenoy G, Zhou F, McGinley R, et al. Effect of airborne contaminants on the wettability of supported graphene and graphite. Nature Materials. 2013;12:925.
[15] Zheng S-F, Gross U, Wang X-D. Dropwise condensation: From fundamentals of wetting, nucleation, and droplet mobility to performance improvement by advanced functional surfaces. Advances in Colloid and Interface Science. 2021;295:102503.
[16] Preston DJ, Miljkovic N, Sack J, Enright R, Queeney J, Wang EN. Effect of hydrocarbon adsorption on the wettability of rare earth oxide ceramics. Appl Phys Lett. 2014;105:011601.
[17] Strohmeier BR. The effects of O2 plasma treatments on the surface composition and wettability of cold-rolled aluminum foil. J Vac Sci Technol. 1989;7:3238-45.
[18] Takeda S, Fukawa M, Hayashi Y, Matsumoto K. Surface OH group governing adsorption properties of metal oxide films. Thin Solid Films. 1999;339:220-4.
[19] Oh J, Orejon D, Park W, Cha H, Sett S, Yokoyama Y, et al. The apparent surface free energy of rare earth oxides is governed by hydrocarbon adsorption. iScience. 2022;25:103691.
[20] Yan X, Huang Z, Sett S, Oh J, Cha H, Li L, et al. Atmosphere-Mediated Superhydrophobicity of Rationally Designed Micro/Nanostructured Surfaces. ACS Nano. 2019;13:4160-73.
[21] Guo H, Ling ZH, Cheng HR, Simpson IJ, Lyu XP, Wang XM, et al. Tropospheric volatile organic compounds in China. Sci Total Environ. 2017;574:1021-43.
[22] González-Gaya B, Fernández-Pinos M-C, Morales L, Méjanelle L, Abad E, Piña B, et al. High atmosphere–ocean exchange of semivolatile aromatic hydrocarbons. Nature Geoscience. 2016;9:438.
[23] McDonald BC, de Gouw JA, Gilman JB, Jathar SH, Akherati A, Cappa CD, et al. Volatile chemical products emerging as largest petrochemical source of urban organic emissions. Science. 2018;359:760-4.
[24] Zhang H, Wang X, Shen X, Li X, Wu B, Li G, et al. Chemical characterization of volatile organic compounds (VOCs) emitted from multiple cooking cuisines and purification efficiency assessments. Journal of Environmental Sciences. 2023;130:163-73.
[25] Sindelarova K, Granier C, Bouarar I, Guenther A, Tilmes S, Stavrakou T, et al. Global data set of biogenic VOC emissions calculated by the MEGAN model over the last 30 years. Atmos Chem Phys. 2014;14:9317-41.
[26] Dani KGS, Loreto F. Trade-Off Between Dimethyl Sulfide and Isoprene Emissions from Marine Phytoplankton. Trends in Plant Science. 2017;22:361-72.
[27] Guenther A, Hewitt CN, Erickson D, Fall R, Geron C, Graedel T, et al. A global model of natural volatile organic compound emissions. J Geophys Res Atmos. 1995;100:8873-92.
[28] Duc NH, Vo HTN, van Doan C, Hamow K, Le KH, Posta K. Volatile organic compounds shape belowground plant-fungi interactions. Frontiers in plant science. 2022;13:1046685.

[29] Al Hallak M, Verdier T, Bertron A, Roques C, Bailly J-D. Fungal Contamination of Building Materials and the Aerosolization of Particles and Toxins in Indoor Air and Their Associated Risks to Health: A Review. Toxins. 2023;15:175.
[30] Gligorovski S, Abbatt JPD. An indoor chemical cocktail. Science. 2018;359:632-3.
[31] Aghababai Beni A, Jabbari H. Nanomaterials for Environmental Applications. Results in Engineering. 2022;15:100467.
[32] Bamford HA, Poster DL, Baker JE. Temperature dependence of Henry's law constants of thirteen polycyclic aromatic hydrocarbons between 4°C AND 31°C. Environ Toxicol Chem. 1999;18:1905-12.
[33] Liu Z, Song Y, Rajappan A, Wang EN, Preston DJ. Temporal Evolution of Surface Contamination under Ultra-high Vacuum. Langmuir. 2022;38:1252-8.
[34] Zhu L, Shen D, Luo KH. A critical review on VOCs adsorption by different porous materials: Species, mechanisms and modification methods. J Hazard Mater. 2020;389:122102.
[35] Orejon D, Askounis A, Takata Y, Attinger D. Dropwise Condensation on Multi-scale Bioinspired Metallic Surfaces with Nano-Features. ACS Appl Mater Interfaces. 2019;11:24735-50.
[36] Adam NK. The Physics and Chemistry of Surfaces. 3d ed. ed. London: Oxford University Press; 1941.
[37] Sutherland KL, Wark IW. Principles of flotation: Melbourne : Australasian Institute of Mining and Metallurgy; 1955.
[38] Fox HW, Hare EF, Zisman WA. Wetting Properties of Organic Liquids on High-Energy Surfaces. The Journal of Physical Chemistry. 1955;59:1097-106.
[39] Gaudin AM. Flotation. New York: McGraw Hill Inc.; 1957.
[40] Bewig KW, Zisman WA. Surface Potentials and Induced Polarization in Nonpolar Liquids Adsorbed on Metals1. The Journal of Physical Chemistry. 1964;68:1804-13.
[41] Bewig KW, Zisman WA. The Wetting of Gold and Platinum by Water. The Journal of Physical Chemistry. 1965;69:4238-42.
[42] White ML. The Wetting of Gold Surfaces by Water1. The Journal of Physical Chemistry. 1964;68:3083-5.
[43] Fowkes FM. Attractive Forces at Interfaces. Industrial & Engineering Chemistry. 1964;56:40-52.
[44] Zisman WA. Relation of the Equilibrium Contact Angle to Liquid and Solid Constitution. Contact Angle, Wettability, and Adhesion. Vol. 43: American Chemical Society 1964. Chapter 1. p. 1-51.
[45] Ma J, Zarin I, Miljkovic N. Direct Measurement of Solid-Liquid Interfacial Energy Using a Meniscus. Physics Review Letters. 2023.
[46] Smith T. The hydrophilic nature of a clean gold surface. Journal of Colloid and Interface Science. 1980;75:51-5.
[47] Westwater JW. Gold surfaces for condensation heat transfer. Gold Bulletin. 1981;14:95-101.
[48] Chakraborty M, Weibel JA, Garimella SV. Tears of an evaporating methanol meniscus on a silicon substrate. Applied Physics Letters. 2018;113:083703.
[49] Orejon D, Sefiane K, Shanahan MER. Stick–Slip of Evaporating Droplets: Substrate Hydrophobicity and Nanoparticle Concentration. Langmuir. 2011;27:12834-43.
[50] Kim MC, Yang SH, Boo JH, Han JG. Surface treatment of metals using an atmospheric pressure plasma jet and their surface characteristics. Surface and Coatings Technology. 2003;174-175:839-44.
[51] Lundy R, Byrne C, Bogan J, Nolan K, Collins MN, Dalton E, et al. Exploring the Role of Adsorption and Surface State on the Hydrophobicity of Rare Earth Oxides. ACS Appl Mater Interfaces. 2017;9:13751-60.
[52] Goswami A, Pillai SC, McGranaghan G. Surface modifications to enhance dropwise condensation. Surfaces and Interfaces. 2021;25:101143.
[53] Mantel M, Wightman JP. Influence of the surface chemistry on the wettability of stainless steel. Surface and Interface Analysis. 1994;21:595-605.
[54] Kokalj A. Corrosion inhibitors: physisorbed or chemisorbed? Corrosion Science. 2022;196:109939.
[55] Agboola OD, Benson NU. Physisorption and Chemisorption Mechanisms Influencing Micro (Nano) Plastics-Organic Chemical Contaminants Interactions: A Review. Frontiers in Environmental Science. 2021;9.
[56] Taborelli M. Cleaning and surface properties. CAS - CERN Accelerator School : Vacuum in Accelerators. 2006:321-40.
[57] Rafiee J, Mi X, Gullapalli H, Thomas AV, Yavari F, Shi Y, et al. Wetting transparency of graphene. Nature Materials. 2012;11:217-22.
[58] Wang H, Orejon D, Song D, Zhang X, McHale G, Takamatsu H, et al. Non-wetting of condensation-induced droplets on smooth monolayer suspended graphene with contact angle approaching 180 degrees. Communications Materials. 2022;3:75.
[59] Furmidge CGL. Studies at phase interfaces. I. The sliding of liquid drops on solid surfaces and a theory for spray retention. Journal of Colloid Science. 1962;17:309-24.

[60] Misiiuk K, Blaikie R, Sommers A, Lowrey S. Force balance model for spontaneous droplet motion on bio-inspired topographical surface tension gradients. Physics of Fluids. 2023;35:024108.
[61] Schnell G, Polley C, Thomas R, Bartling S, Wagner J, Springer A, et al. How droplets move on laser-structured surfaces: Determination of droplet adhesion forces on nano- and microstructured surfaces. Journal of Colloid and Interface Science. 2023;630:951-64.
[62] Carre A, Shanahan MER. Drop Motion on an Inclined Plane and Evaluation of Hydrophobia Treatments to Glass. The Journal of Adhesion. 1995;49:177-85.
[63] Tao R, McHale G, Reboud J, Cooper JM, Torun H, Luo J, et al. Hierarchical Nanotexturing Enables Acoustofluidics on Slippery yet Sticky, Flexible Surfaces. Nano Letters. 2020;20:3263-70.
[64] Gulfam R, Orejon D, Choi C-H, Zhang P. Phase-Change Slippery Liquid-Infused Porous Surfaces with Thermo-Responsive Wetting and Shedding States. ACS Applied Materials & Interfaces. 2020;12:34306-16.
[65] Lv F, Zhao F, Cheng D, Dong Z, Jia H, Xiao X, et al. Bioinspired functional SLIPSs and wettability gradient surfaces and their synergistic cooperation and opportunities for enhanced condensate and fluid transport. Advances in Colloid and Interface Science. 2022;299:102564.
[66] McHale G, Gao N, Wells GG, Barrio-Zhang H, Ledesma-Aguilar R. Friction Coefficients for Droplets on Solids: The Liquid–Solid Amontons' Laws. Langmuir. 2022;38:4425-33.
[67] Gao N, Geyer F, Pilat DW, Wooh S, Vollmer D, Butt H-J, et al. How drops start sliding over solid surfaces. Nature Physics. 2017;14:191.
[68] Cassie ABD, Baxter S. Wettability of porous surfaces. Transactions of the Faraday Society. 1944;40:546-51.
[69] Raj R, Enright R, Zhu Y, Adera S, Wang EN. Unified Model for Contact Angle Hysteresis on Heterogeneous and Superhydrophobic Surfaces. Langmuir. 2012;28:15777-88.
[70] Israelachvili JN, Gee ML. Contact angles on chemically heterogeneous surfaces. Langmuir. 1989;5:288-9.
[71] Mall ID, Srivastava VC, Agarwal NK, Mishra IM. Adsorptive removal of malachite green dye from aqueous solution by bagasse fly ash and activated carbon-kinetic study and equilibrium isotherm analyses. Colloids and Surfaces A: Physicochemical and Engineering Aspects. 2005;264:17-28.
[72] Ho Y-S. Review of second-order models for adsorption systems. Journal of Hazardous Materials. 2006;136:681-9.
[73] Ho YS, McKay G. Pseudo-second order model for sorption processes. Process Biochemistry. 1999;34:451-65.
[74] Tan KL, Hameed BH. Insight into the adsorption kinetics models for the removal of contaminants from aqueous solutions. Journal of the Taiwan Institute of Chemical Engineers. 2017;74:25-48.
[75] Lagergren S. Zur theorie der sogenannten adsorption geloster stoffe. Kungliga Svenska Vetenskapsakademiens Handlingar. 1898;24:1-39.
[76] Yan X, Chen F, Zhang X, Qin Y, Zhao C, Sett S, et al. Atmosphere-Mediated Scalable and Durable Biphilicity on Rationally Designed Structured Surfaces. Advanced Materials Interfaces. 2020;7:2000475.
[77] Li J, Zhao Y, Ma J, Fu W, Yan X, Rabbi KF, et al. Superior Antidegeneration Hierarchical Nanoengineered Wicking Surfaces for Boiling Enhancement. Advanced Functional Materials. 2022;32:2108836.
[78] Cha H, Wu A, Kim M-K, Saigusa K, Liu A, Miljkovic N. Nanoscale-Agglomerate-Mediated Heterogeneous Nucleation. Nano Letters. 2017;17:7544-51.
[79] Yu X, Dorao CA, Fernandino M. Droplet evaporation during dropwise condensation due to deposited volatile organic compounds. AIP Advances. 2021;11.
[80] Chang H, Liu B, Zhang Z, Pawar R, Yan Z, Crittenden JC, et al. A Critical Review of Membrane Wettability in Membrane Distillation from the Perspective of Interfacial Interactions. Environmental Science & Technology. 2021;55:1395-418.
[81] Lu Y, Wang S, Huang G, Xi L, Qin G, Zhu M, et al. Fabrication and applications of the optical diamond-like carbon films: a review. Journal of Materials Science. 2022;57:3971-92.
[82] Xie J, Zhang J, Zhang X, Guo Z, Hu Y. Durable multifunctional superhydrophobic sponge for oil/water separation and adsorption of volatile organic compounds. Research on Chemical Intermediates. 2020;46:4297-309.
[83] Zhao L, Li Y, Yu M, Peng Y, Ran F. Electrolyte-Wettability Issues and Challenges of Electrode Materials in Electrochemical Energy Storage, Energy Conversion, and Beyond. Advanced Science. 2023;10:2300283.
[84] Song S, Zhang S, Zhang X, Verma P, Wen M. Advances in Catalytic Oxidation of Volatile Organic Compounds over Pd-Supported Catalysts: Recent Trends and Challenges. Frontiers in Materials. 2020;7.
[85] Zhou X, Zheng Y, Shimizu T, Euaruksakul C, Tunmee S, Wang T, et al. Colorful Diamond-Like Carbon Films from Different Micro/Nanostructures. Advanced Optical Materials. 2020;8:1902064.

[86] Meng K, Yu L, Jing S, Tan X, Chen X, Wang G. Microstructures, mechanical properties and surface wettability of La-doped diamond-like carbon films deposited by magnetron co-sputtering. Journal of Alloys and Compounds. 2023;934:167860.
[87] Song Y, Zhang L, Liu Z, Preston DJ, Wang EN. Effects of airborne hydrocarbon adsorption on pool boiling heat transfer. Applied Physics Letters. 2020;116.
[88] McHale G, Afify N, Armstrong S, Wells GG, Ledesma-Aguilar R. The Liquid Young's Law on SLIPS: Liquid–Liquid Interfacial Tensions and Zisman Plots. Langmuir. 2022;38:10032-42.
[89] Owens DK, Wendt RC. Estimation of the surface free energy of polymers. Journal of Applied Polymer Science. 1969;13:1741-7.
[90] Kaelble DH. Dispersion-Polar Surface Tension Properties of Organic Solids. The Journal of Adhesion. 1970;2:66-81.
[91] Rabel W. Einige Aspekte der Benetzungstheorie and ihre Anwendung auf die Untersuchung and Veränderung der Oberflächeneigenschaften von Polymeren. Farbe and Lack. 1971;77:997-1005.
[92] Sarkar S, Jafari Gukeh M, Roy T, Gaikwad H, Bellussi FM, Moitra S, et al. A new methodology for measuring solid/liquid interfacial energy. Journal of Colloid and Interface Science. 2023;633:800-7.
[93] Chang F-M, Cheng S-L, Hong S-J, Sheng Y-J, Tsao H-K. Superhydrophilicity to superhydrophobicity transition of CuO nanowire films. Applied Physics Letters. 2010;96.
[94] Shirazy MRS, Blais S, Fréchette LG. Mechanism of wettability transition in copper metal foams: From superhydrophilic to hydrophobic. Applied Surface Science. 2012;258:6416-24.
[95] Wang G, Zhang T-Y. Oxygen adsorption induced superhydrophilic-to-superhydrophobic transition on hierarchical nanostructured CuO surface. Journal of Colloid and Interface Science. 2012;377:438-41.
[96] Upot NV, Fazle Rabbi K, Khodakarami S, Ho JY, Kohler Mendizabal J, Miljkovic N. Advances in micro and nanoengineered surfaces for enhancing boiling and condensation heat transfer: a review. Nanoscale Advances. 2023;5:1232-70.
[97] Cao Z, Ouyang Z, Liu Z, Li Y, Ouyang Y, Lin J, et al. Effects of surface oxides and nanostructures on the spontaneous wettability transition of laser-textured copper surfaces. Applied Surface Science. 2021;560:150021.
[98] Gomollón-Bel F. IUPAC Top Ten Emerging Technologies in Chemistry 2021. Breakthroughs for a circular, climate-neutral future. 2021;43:13-20.
[99] Liu Z, Yap TF, Rajappan A, Shveda R, Rasheed R, Preston DJ. Mitigating Contamination with Nanostructure-Enabled Ultra-Clean Storage. Nano Letters. 2023;(Under Review).
[100] Carpenter J, Kim H, Suarez J, van der Zande A, Miljkovic N. The Surface Energy of Hydrogenated and Fluorinated Graphene. ACS Applied Materials & Interfaces. 2023;15:2429-36.
[101] Wan H, Li S, Li J, Liu T, Lin J, Min J. Wettability transition of metallic surfaces from laser-generated superhydrophilicity to water-induced superhydrophobicity via a facile and eco-friendly strategy. Materials & Design. 2023;226:111691.
[102] Shi Z, Zhang Z, Huang W, Zeng H, Mandić V, Hu X, et al. Spontaneous Adsorption-Induced Salvinia-like Micropillars with High Adhesion. Langmuir. 2021;37:6728-35.
[103] Mousa MH, Günay AA, Orejon D, Khodakarami S, Nawaz K, Miljkovic N. Gas-Phase Temperature Mapping of Evaporating Microdroplets. ACS Applied Materials & Interfaces. 2021;13:15925-38.
[104] Guo X, Li X, Gan G, Wang L, Fan S, Wang P, et al. Functionalized Activated Carbon for Competing Adsorption of Volatile Organic Compounds and Water. ACS Applied Materials & Interfaces. 2021;13:56510-8.
[105] Kujawa J, Zięba M, Zięba W, Al-Gharabli S, Kujawski W, Terzyk AP. Hedgehog-like structure, PVDF-carbon nanohorn hybrid membranes for improved removal of VOCs from water. Chemical Engineering Journal. 2022;438:135574.
[106] Ma J, Cha H, Kim M-K, Cahill DG, Miljkovic N. Condensation Induced Delamination of Nanoscale Hydrophobic Films. Advanced Functional Materials. 2019;29:1905222.
[107] K. P. Veerapandian S, De Geyter N, Giraudon J-M, Lamonier J-F, Morent R. The Use of Zeolites for VOCs Abatement by Combining Non-Thermal Plasma, Adsorption, and/or Catalysis: A Review. Catalysts. 2019;9:98.
[108] Yu B, Deng H, Lu Y, Pan T, Shan W, He H. Adsorptive interaction between typical VOCs and various topological zeolites: Mixture effect and mechanism. Journal of Environmental Sciences. 2024;136:626-36.
[109] Kim T, Sohn S, Park H, Jang S, Lee C, Lee JI, et al. Surface-dependent gas equilibrium of semi-volatile organic compounds on glass, wood, and polyurethane foam using SPME-GC/MS. Chemosphere. 2022;291:132869.